1994-06

Analysis of direct detection lightwave systems with optical amplifiers

Kucukerman, Enver

Monterey, California. Naval Postgraduate School

NAVAL POSTGRADUATE SCHOOL
Monterey, California

THESIS

Analysis of Direct Detection Lightwave Systems with Optical Amplifiers

by

Enver Kucukerman

June 1994

Thesis Advisor: Tri T. Ha

Approved for public release, distribution is unlimited.

REPORT DOCUMENTATION PAGE

Form Approved
OMB No. 0704-0188

1. AGENCY USE ONLY (Leave blank)	2. REPORT DATE	3. REPORT TYPE AND DATES COVERED
	June 1994	Master's Thesis

4. TITLE AND SUBTITLE
ANALYSIS OF DIRECT DETECTION LIGHTWAVE SYSTEMS WITH OPTICAL AMPLIFIERS

5. FUNDING NUMBERS

6. AUTHOR(S)
Kucukerman, Enver

7. PERFORMING ORGANIZATION NAME(S) AND ADDRESS(ES)
Naval Postgraduate School
Monterey, CA 93943-5000

8. PERFORMING ORGANIZATION REPORT NUMBER

9. SPONSORING/MONITORING AGENCY NAME(S) AND ADDRESS(ES)

10. SPONSORING/MONITORING AGENCY REPORT NUMBER

11. SUPPLEMENTARY NOTES
The views expressed in this thesis are those of the author and do not reflect the official policy or position of the Department of Defense or the United States Government.

12a. DISTRIBUTION/AVAILABILITY STATEMENT
Approved for public release; distribution unlimited.

12b. DISTRIBUTION CODE

13. ABSTRACT *(Maximum 200 words)*

We provide a detailed analysis of direct detection lightwave systems employing an optical preamplifier at the receiver and derive the closed form expression for the bit error probability of WDM systems employing on-off keying (OOK) as modulation format. In our analysis, we consider various cases in which the receiver model uses either a finite-time integrator or Fabry-Perot filter operating in a single channel or multi-channel environment. We take into account the optical amplifier noise, the postdetection receiver noise, the shot noise, and the effect of the nonzero laser linewidth.

14. SUBJECT TERMS	15. NUMBER OF PAGES
FSR, responsivity, ACI, ISI,	77
	16. PRICE CODE

17. SECURITY CLASSIFICATION OF REPORT	18. SECURITY CLASSIFICATION OF THIS PAGE	19. SECURITY CLASSIFICATION OF ABSTRACT	20. LIMITATION OF ABSTRACT
UNCLASSIFIED	UNCLASSIFIED	UNCLASSIFIED	UL

Approved for public release; distribution is unlimited

Analysis of Direct Detection Lightwave Systems with Optical Amplifiers

by

Enver Kucukerman
Lieutenant Junior Grade, Turkish Navy
B. S., Turkish Naval Academy, 1988

Submitted in partial fulfillment of the
requirements for the degree of

MASTER OF SCIENCE IN ELECTRICAL ENGINEERING

from the

NAVAL POSTGRADUATE SCHOOL

June 1994

Author: [redacted]
Enver Kucukerman

Approved by: [redacted]
Tri T. Ha, Thesis Advisor

[redacted]
Randy L. Borchardt, Co-Advisor

[redacted]
Michael A. Morgan, Chairman, Department of Electrical
and Computer Engineering

ABSTRACT

We provide a detailed analysis of direct detection lightwave systems employing an optical preamplifier at the receiver a[illegible]ive the closed form expression for the bit error probability of WDM systems employing on-off keying (OOK) as modulation format. In our analysis, we consider various cases in which the receiver model uses either a finite-time integrator or Fabry-Perot filter operating in a single channel or multi-channel environment. We take into account the optical amplifier noise, the postdetection receiver noise, the shot noise, and the effect of the nonzero laser linewidth.

TABLE OF CONTENTS

LIST OF TABLES

LIST OF FIGURES

I. INTRODUCTION

Current development of optical amplifiers has advanced to the stage that their widespread use in lightwave systems is certain in the near future [1]. Receivers using optical amplifiers have been shown to be substantially more sensitive than their counterparts [2]. Of primary importance is the use of the optical amplifier as a preamplifier in a direct detection receiver. In this study, a unified approach to the performance evaluation of direct detection on-off keying (OOK) lightwave systems which take into account the effect of postdetection thermal noise, shot noise, and the impact of nonzero laser linewidth is provided.

The direct detection OOK receiver to be analyzed is shown in Fig. 1. The received signal is amplified by an optical amplifier of gain G. The optical amplifier introduces additive white Gaussian noise (AWGN) with zero mean and power spectral density (PSD) $N_0/2$ where $N_0 = N_{sp}hf(G-1)$ [2, 12, 33]. The parameter N_{sp} represents the spontaneous emission factor which is unity for an ideal amplifier, h is Planck's constant (6.626×10^{-34} J.s), and f is the frequency. Because the optical amplifier is not polarization independent, a polarizer is needed to pass the desired signal and to block the light in the orthogonal polarization. In this study, the optical bandpass filter is modeled by both a finite-time bandpass integrator with integration time T' [6, 9–11, 33] and a Fabry-Perot filter.

For the finite-time integrator, the noise bandwidth $1/T'$ of the bandpass integrator is chosen to be the same as the noise bandwidth of the optical filter. The equivalent lowpass impulse response of the integrator is $h(t) = (1/T')[u(t)-u(t-T')]$ where $u(t)$ is the unit step function. For convenience of analysis, it is assumed that the bit duration T is a multiple integer of T', that is, $T = MT'$ [33].

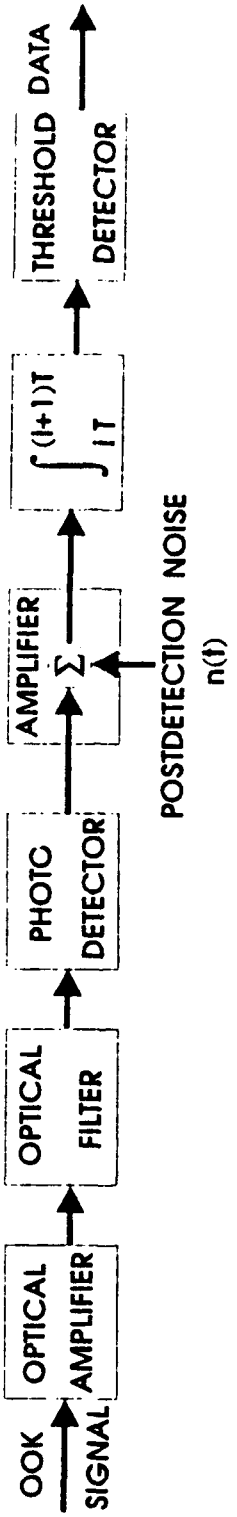

Figure 1: OOK receiver structure.

The photodiode has a responsivity $R = \eta_e q/hf$ where $\eta_e \leq 1$ is the quantum efficiency and q is the electron charge (1.6×10^{-19} C). The output current of the photodiode, which is proportional to the squared envelope of the receiver signal, is processed by a detector which consists of a low noise amplifier, an integrate-and-dump filter and a slicer [33].

In the case where a finite time integrator is employed, the amplifier noise effect is most pronounced at low postdetection thermal noise. With a higher gain, the amplifier noise is dominant and, consequently, the net amplifier gain is reduced considerably. In the case where a Fabry-Perot filter is employed as an optical filter at the receiver model, the equivalent lowpass impulse response of the Fabry-Perot filter can be well approximated by an RC filter for both single and multi-channel within the frequency range $|f - f_0| < FSR/20\pi$ where FSR is the free spectral range and f_0 is the center frequency of the Fabry-Perot filter. For example, given $FSR = 3800$ GHz, the approximation works very well for $|f - f_0| < 60.5$ GHz. In other words, the effects of adjacent channels within 121 GHz can be included. The same model without the optical amplifier is analyzed in [29] and it is seen that this model enables use to obtain a closed form analytical expression for the bit error probability. In all bit error probability derivations, whether a finite-time integrator or a Fabry-Perot filter is employed as the optical filter in the receiver model, it is assumed that all channels are bit synchronous as in [29, 30].

This thesis is organized into three sections. In the second section, the receiver models employing finite-time integrator, and the analysis is a reproduction of [33], Fabry-Perot filter for single channel and Fabry-Perot filter for multi-channel are analyzed. Each of these analyses obtain the mathematical framework, bit error probability, and the numerical results deriving the detected signal envelope and its density function. The last section provides the conclusions.

[THIS PAGE INTENTIONALLY LEFT BLANK]

II. ANALYSIS

The analysis is organized into three subsections. All three provide the mathematical framework, bit error probability derived from the statistics of the white Gaussian postdetection thermal noise and the numerical results for the receiver model considered. The receiver model to be analyzed is shown in Fig. 1.

A. FINITE-TIME INTEGRATOR MODEL

The optical bandpass filter is modeled as a finite time bandpass integrator with integration time T'. The noise bandwidth $1/T'$ of the bandpass integrator is chosen to be the same as the noise bandwidth of the optical filter. This model is used because it is analytically tractable. This section is taken from [33].

1. Mathematical Framework

For mathematical convenience we adopt the complex envelope notation of a real OOK signal. Thus, for a given transmitted bit b_i the corresponding received signal at the input of the optical bandpass filter in Fig. 1 is designated as follows:

$$r_i(t) = \sqrt{GP}\, b_i e^{j\theta(t)} p_T(t) + n_c(t) + j n_s(t) \tag{1}$$

where $p_T = 1, 0 < t < T$ and zero otherwise, G is the optical amplifier gain, P is the peak power at the input of the optical amplifier, $\theta(t)$ is the OOK laser phase noise, and $n_c(t)$ and $n_s(t)$ are the independent in-phase and quadrature components of the additive zero mean white Gaussian noise representing the amplifier spontaneous emission noise. The PSD of $n_c(t)$ and $n_s(t)$ is $N_0/2$ (we use $N_0/2$ instead of the usual lowpass PSD N_0 because the magnitude of the signal component is $\sqrt{GP}\, b_i$ instead of the usual $\sqrt{2GP}\, b_i$ for complex envelope). Let r be the extinction ratio of the laser source defined as the ratio of the transmitted power for the logical zero to that

for the logical one. Then $b_0 = \sqrt{r/(1+r)}$ for the logical zero, and $b_1 = \sqrt{1/(1+r)}$ for the logical one.

a. Approximation of the Detected Signal Envelope

The output signal of the optical bandpass filter is given by

$$\begin{aligned} s_i(t) &= \frac{1}{T'}\int_{-\infty}^{\infty}[u(\tau)-u(\tau-T']r_i(t-\tau)d\tau \\ &= \frac{1}{T'}\int_0^{T'} r_i(t-\tau)d\tau \\ &= \frac{1}{T'}\int_{t-T'}^{t} r_i(\tau)d\tau \end{aligned} \tag{2}$$

The photodetector with responsivity R detects the squared envelope $R|s_i(t)|^2$. This signal current plus the shot noise current $v_i(t)$ generated by the photodiode, and the postdetection thermal noise current $w(t)$ are scaled by $1/TRGP$ and integrated to produce the decision variable

$$\begin{aligned} Y_i &= \frac{1}{TRGP}\int_0^T R|s_i(t)|^2dt + \frac{1}{TRGP}\int_0^T v_i(t)dt \\ &\quad + \frac{1}{TRGP}\int_0^T w(t)dt \\ &= X_i + V_i + W \end{aligned} \tag{3}$$

where

$$X_i = \frac{1}{TRGP}\int_0^T R|s_i(t)|^2dt \tag{4}$$

$$V_i = \frac{1}{TRGP}\int_0^T v_i(t)dt \tag{5}$$

$$W = \frac{1}{TRGP}\int_0^T w(t)dt \tag{6}$$

We model $w(t)$ as a zero mean white Gaussian noise current of spectral density W_0. It is seen that the variance of σ_W^2 of $w(t)$ is

$$\sigma_W^2 = \frac{W_0}{TR^2G^2P^2} \tag{7}$$

The shot noise current $v_i(t)$ can be modeled as a zero mean Gaussian noise current with spectral density V_{0i} as follows [15]:

$$V_{0i} = qRE\{|s_i(t)|^2\} \tag{8}$$

The variance $\sigma_{V_i}^2$ of $v_i(t)$ is thus given by

$$\sigma_{V_i}^2 = \frac{q}{TRG^2P^2} E\{|s_i(t)|^2\} \tag{9}$$

The value of $\sigma_{V_i}^2$ can be computed from (A1) and (A4) as follows:

$$\sigma_{V_i}^2 = \frac{2qM^2b_i^2}{TRGP(\pi\beta T)^2}\left(\frac{\pi\beta T}{M} + e^{-\pi\beta T/M} - 1\right) + \frac{qMN_{sp}hf(G-1)}{T^2RG^2P^2} \tag{10}$$

where β is the laser linewidth.

The statistics of X_i are very difficult to obtain. Therefore, we make the following approximation of X_i. We note that the equivalent lowpass impulse response $h(t)$ of the optical bandpass filter is assumed to be time-limited to $T' = T/M$. Thus, the integrand $R|s_i(kT')|^2$, $k = 1, 2, \cdots, M$ in (4) is evaluated at $t = kT'$ where there are k independent and identically distributed (iid) samples of $R|s_i(t)|^2$ during an interval T. Thus $|s_i(kT')|^2$ is obtained from disjoint integration intervals where the phase noise $\theta(t)$ has independent increments and the noise $n_c(t)$ and $n_s(t)$ are altogether independent over disjoint intervals. Using the above fact we can approximate X_i as the sum of M iid samples $T'R|s_i(kT')|^2/TRGP$. That is

$$X_i \approx \frac{1}{MGP}\sum_{k=1}^{M}|s_i(kT')|^2 \tag{11}$$

Substituting (1)–(2) into (11) we obtain

$$X_i \approx \sum_{k=1}^{M}\left|\frac{b_iZ_k}{\sqrt{M}} + N_{ck} + jN_{sk}\right|^2 \tag{12}$$

where

$$Z_k = \frac{1}{T'}\int_{(k-1)T'}^{kT'} e^{j\theta(t)}dt \tag{13}$$

$$N_{ck} = \frac{1}{T'\sqrt{MGP}} \int_{(k-1)T'}^{kT'} n_c(t)dt \tag{14}$$

$$N_{sk} = \frac{1}{T'\sqrt{MGP}} \int_{(k-1)T'}^{kT'} n_s(t)dt \tag{15}$$

The random variables N_{ck} and N_{sk} are independent Gaussian random variables with zero mean and variance σ^2 given by

$$\sigma^2 = \frac{N_0}{2TGP} = \frac{N_{sp}hf(G-1)}{2TGP} \tag{16}$$

The approximation of X_i in (12) is equivalent to the modeling of the integrate-and-dump filter as a discrete-time integration that sums over M samples taken every T' seconds at the output of the photodetector [6, 13]. We remark that both X_i and its approximation have the same mean value. If $|s_i(t)|^2$ has a constant spectral density, then X_i and its approximation also have the same variance. This happens when M is large and the spectral density of $|s_i(t)|^2$ can be considered constant within the bandwidth $1/T$ of the integrate-and-dump filter.

b. Probability Density Function of the Detected Signal Envelope

From (11) we observe that X_i is approximated by the sum of squares of $2M$ iid Gaussian random variables. Therefore, X_i is approximately noncentral chi-square distributed with the following conditional probability density function (pdf) $f_{X_i}(x_i|\gamma)$ [18]

$$\begin{aligned} f_{X_i}(x_i|\gamma) &= \frac{1}{2\sigma^2}\left(\frac{x_i}{b_i^2\gamma/M}\right)^{(M-1)/2} \exp\left\{-\frac{x_i + b_i^2\gamma/M}{2\sigma^2}\right\} \\ &\quad I_{M-1}\left(\frac{\sqrt{b_i^2\gamma x_i/M}}{\sigma^2}\right) \\ &= \frac{TGP}{N_{sp}hf(G-1)}\left(\frac{Mx_i}{b_i^2\gamma}\right)^{(M-1)/2} \exp\left\{-\frac{TGP(x_i^2 + b_i^2\gamma/M)}{N_{sp}hf(G-1)}\right\} \end{aligned}$$

$$I_{M-1}\left(\frac{2TGP\sqrt{b_i^2\gamma x_i/M}}{N_{sp}hf(G-1)}\right) \tag{17}$$

where $I_{M-1}(\cdot)$ is the modified Bessel function of order $M-1$, and γ is the value assumed by the random variable defined as follows:

$$\Gamma = \sum_{k=1}^{M} |Z_k|^2 \tag{18}$$

In the special case when the extinction ratio $r = 0$, then $b_0 = 0$, and $f_{X_0}(x_0)$ in (17) is a chi-square probability density function (pdf) given by [18]

$$f_{X_0}(x_0) = \frac{1}{(M-1)!}\left(\frac{TGP}{N_{sp}hf(G-1)}\right)^M x_0^{M-1}\exp\left\{-\frac{TGPx_0}{N_{sp}hf(G-1)}\right\} \tag{19}$$

The pdf of $f_{X_i}(x_i|\gamma)$ can be obtained by averaging $f_{X_i}(x_i|\gamma)$ over γ. Thus knowing $f_\Gamma(\gamma)$ we get

$$f_{X_i}(x_i) = \int_0^\infty f_{X_i}(x_i|\gamma) f_\Gamma(\gamma) d\gamma \tag{20}$$

2. Bit Error Probability

For a detection threshold α, the bit error probability conditional on the mean x_0 and x_1 assuming a combined shot noise current and postdetection thermal noise current spectral density $V_{0i} + W_0$ is given by

$$P_b(x_0, x_1) = \frac{1}{4}erfc\left(\frac{\alpha - x_0}{\sqrt{2}\,\sigma_{Y_0}}\right) + \frac{1}{4}erfc\left(\frac{x_1 - \alpha}{\sqrt{2}\,\sigma_{Y_1}}\right) \tag{21}$$

where the complimentary error function $erfc(\cdot)$ is defined as

$$erfc(a) = \frac{2}{\sqrt{\pi}}\int_a^\infty e^{-x^2}dx \tag{22}$$

and $\sigma_{Y_i}^2$, $i = 0, 1$ are the variances of Y_i in (3)

$$\begin{aligned}\sigma_{Y_i}^2 &= \sigma_{V_i}^2 + \sigma_W^2 \\ &= \frac{q}{TRG^2P^2}E\{|s_i(t)|^2\} + \frac{W_o}{TR^2G^2P^2}\end{aligned} \tag{23}$$

The bit error probability P_b is obtained by taking the expectation of $P_b(x_0, x_1)$ with respect to x_0 and x_1 by using (17)

$$P_b = \frac{1}{4}\int_0^\infty erfc\left(\frac{\alpha - x_0}{\sqrt{2}\,\sigma_{Y_0}}\right) f_{X_0}(x_0)dx_0 + \frac{1}{4}\int_0^\infty erfc\left(\frac{x_1 - \alpha}{\sqrt{2}\,\sigma_{Y_1}}\right) f_{X_1}(x_1)dx_1 \tag{24}$$

The optimal threshold that minimizes the bit error probability is the value that satisfies the following equation

$$\int_0^\infty erfc\left(\frac{\alpha - x_0}{\sqrt{2}\sigma_{Y_0}}\right) f_{X_0}(x_0)dx_0 = \int_0^\infty erfc\left(\frac{x_1 - x}{\sqrt{2}\,\sigma_{Y_1}}\right) f_{X_1}(x_1)dx_1 \tag{25}$$

From the above analysis it is seen that the evaluation of the bit error probability P_b requires the knowledge of the pdf $f_\Gamma(\gamma)$ of Γ in (18) which in turn requires the pdf of $|Z_k|^2$ in (13). The pdf of the random variable $|Z_k|^2$ has been studied extensively in [13, 14], [20, 21]. The evaluation of P_b in (24) is computer intensive even in the ideal case of no laser phase noise. When laser phase noise is taken into account, the pdf of Γ must be obtained from the pdf of $|Z_k|^2$ via an M-fold convolution.

3. Numerical Results

In this section we present numerical results for a direct detection lightwave system with the following parameters: $r = 0.05$, $1/T = 500$ Mb/s, $G = 100$ and 1000, and $W_0 = 10^{-24}$, 10^{-23}, 10^{-22} (A^2/Hz). Figure 2 shows the bit error probability P_b versus the input power P (dBW) as a function of postdetection noise spectral density W_0 for a receiver without the filter and the optical amplifier. Figure 3 shows P_b versus P for $G = 100$, $M = 10$ without phase noise and with phase noise of $\beta T = 1$ as a function of W_0. At $P_b = 10^{-15}$, the net amplifier gain without (with) phase noise is 19.6 dB (19 dB) for $W_0 = 10^{-22}$ A^2/Hz, 18.6 (18 dB) for $W_0 = 10^{-23}$ A^2/Hz, and 16.3 dB (15.7 dB) for $W_0 = 10^{-24}$ A^2/Hz. It is seen that the amplifier noise effect is most pronounced at low postdetection noise.

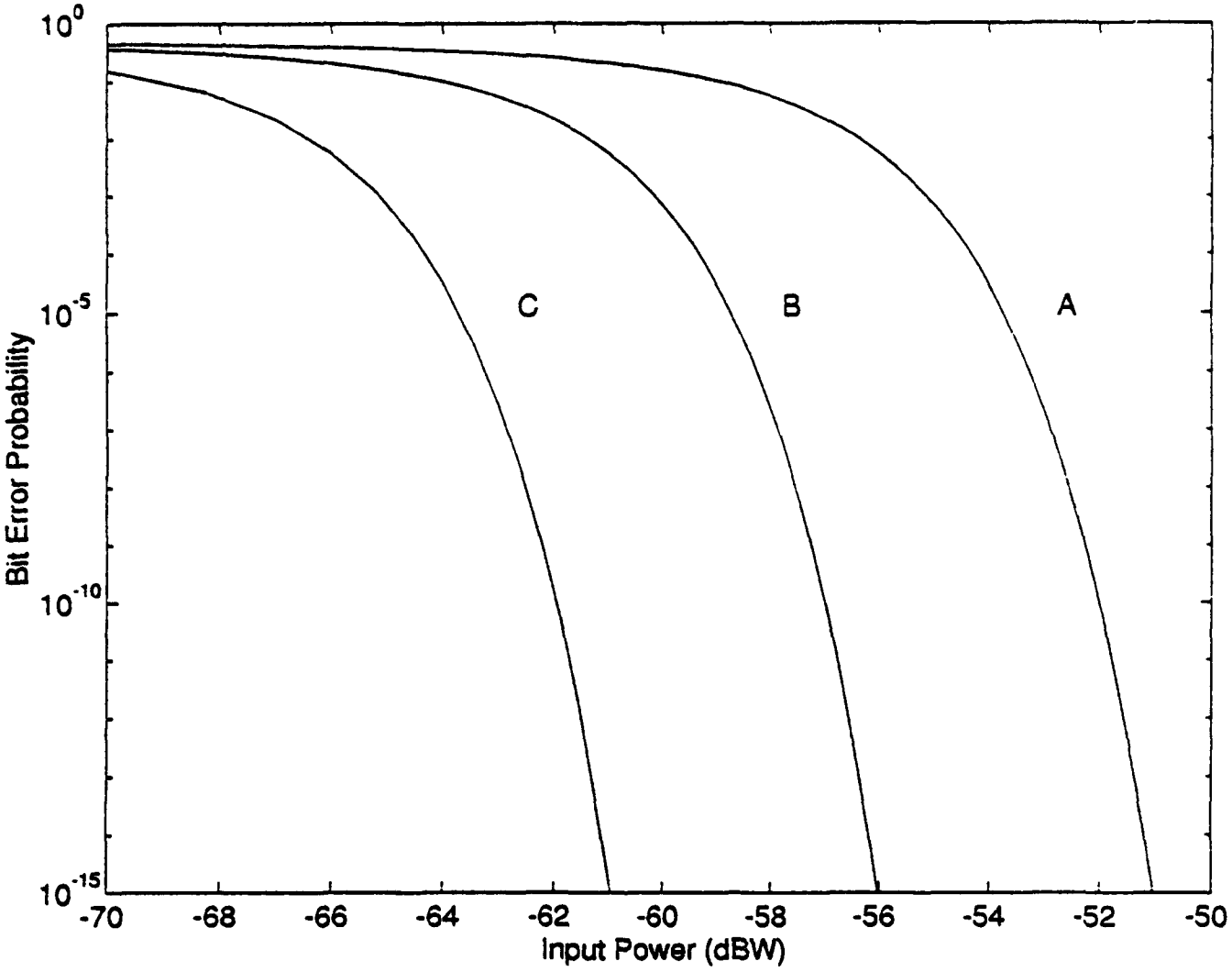

Figure 2: Bit error probability versus input power for a system without optical amplifier as a function of postdetection noise spectral density W_0. A: $W_0 = 10^{-22}$ A^2/Hz, B: $W_0 = 10^{-23}$ A^2/Hz, C: $W_0 = 10^{-24}$ A^2/Hz.

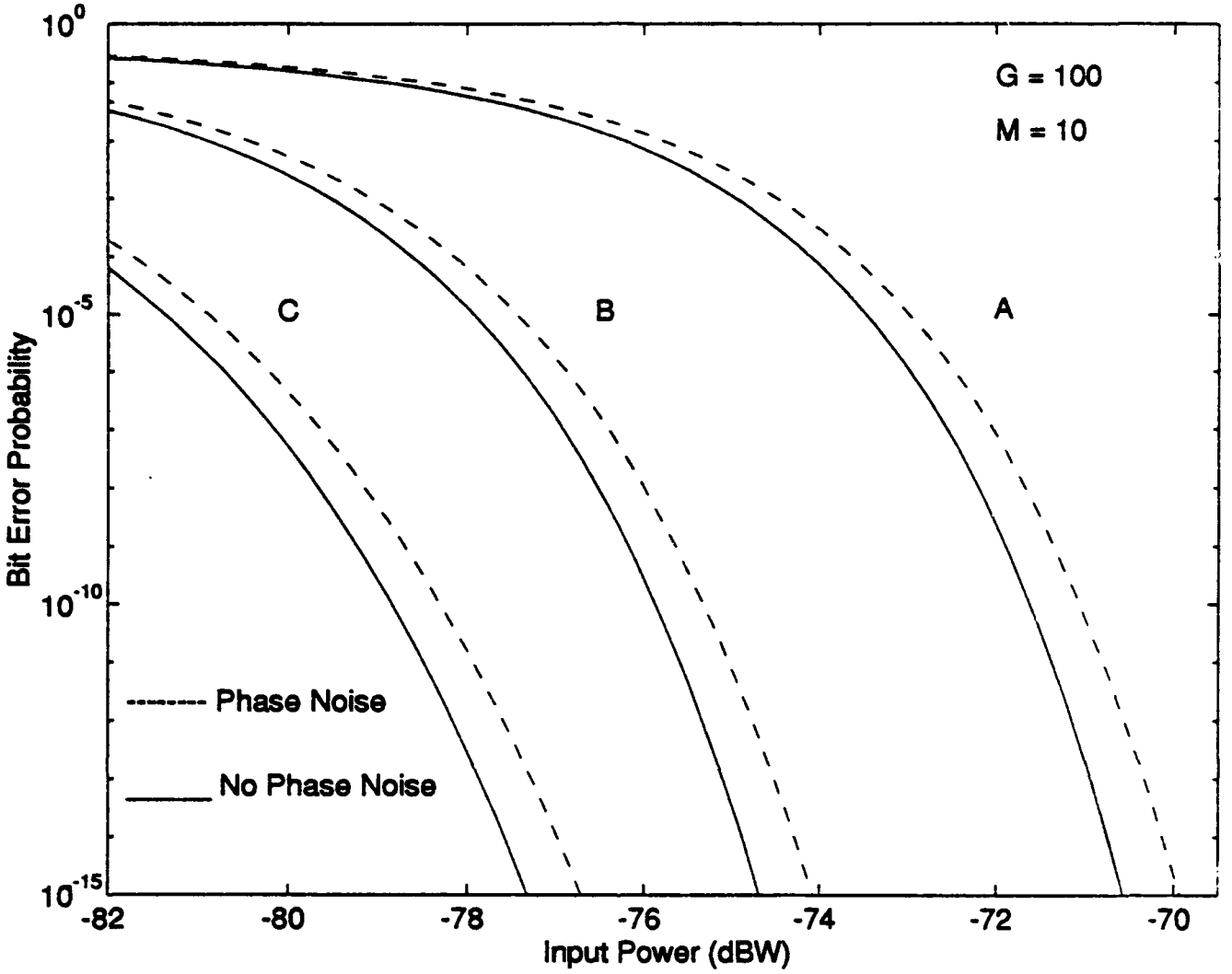

Figure 3: Bit error probability versus input power as a function of postdetection noise spectral density W_0 with $G = 100$, $M = 10$. A: $W_0 = 10^{-22}$ A^2/Hz, B: $W_0 = 10^{-23}$ A^2/Hz, C: $W_0 = 10^{-24}$ A^2/Hz.

Figure 4 shows P_b versus P for $G = 1000$, $M = 10$ without phase noise as a function of W_0. At $P_b = 10^{-15}$, the net amplifier gain is 26.4 dB at $W_0 = 10^{-22}$ A^2/Hz, 22.1 dB at $W_0 = 10^{-23}$ A^2/Hz, and 17.2 dB at $W_0 = 10^{-24}$ A^2/Hz. It is seen that with a higher gain, the amplifier noise is dominant and consequently, the net amplifier gain is reduced considerably. Comparing the two systems that employ optical amplifiers with gain $G = 100$, and $G = 1000$, respectively, we observe that there is a net improvement of 6.8 dB at $W_0 = 10^{-22}$ A^2/Hz, 3.5 dB at $W_0 = 10^{-23}$ A^2/Hz and only 0.9 dB at $W_0 = 10^{-24}$ A^2/Hz for $G = 1000$ over $G = 100$. Besides that, Fig. 5 shows the optimized threshold versus input power P for $G = 100$, $M = 10$, 30, 50, and 100. As it is described in (25), the optimal threshold that minimizes the bit error probability is the value that satisfies the equation given in (25). As we can see from Fig. 5, optimized threshold value decreases as input power increases for all M values. For considered values of M, which are 10, 30, 50, and 100, the optimized threshold appears to converge to about 0.5 for higher input power values. We conclude that a larger gain amplifier should be used when the postdetection noise is large, and a smaller gain amplifier should be used when the postdetection noise is small.

B. FABRY-PEROT FILTER FOR SINGLE CHANNEL

The desired signal is amplified by a preamplifier and then filtered by using a Fabry-Perot filter. The photodetector has a responsivity R (A/W). The detected current is amplified by a low noise amplifier that adds a postdetection thermal noise with spectral density N_0 (A^2/Hz). The decision variable at the output of the integration is compared to the threshold in order to be able to determine whether a bit zero or bit one is present.

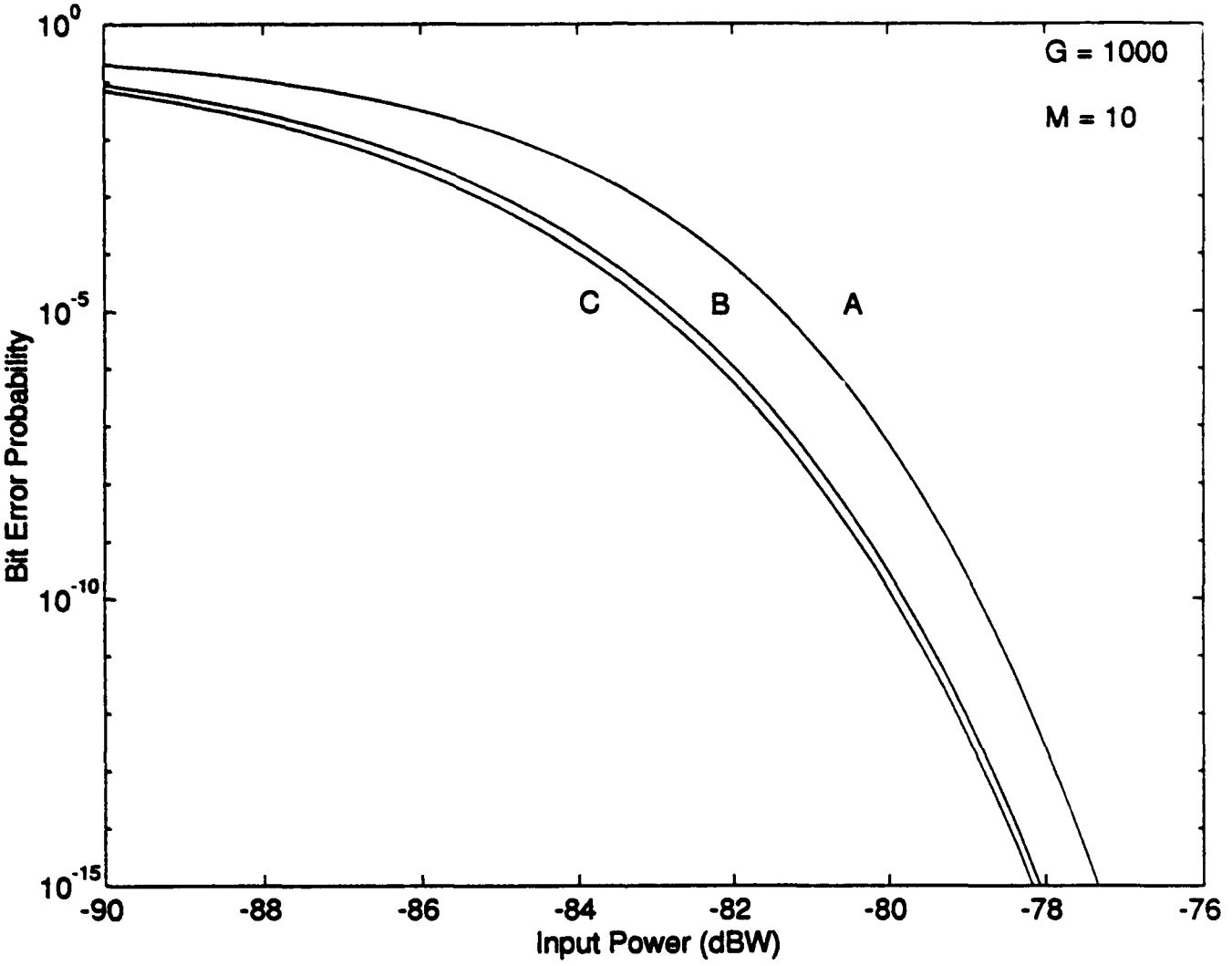

Figure 4: Bit error probability versus input power as a function of postdetection noise spectral density W_0 with $G = 1000$, $M = 10$. A: $W_0 = 10^{-22}$ A^2/Hz, B: $W_0 = 10^{-23}$ A^2/Hz, C: $W_0 = 10^{-24}$ A^2/Hz.

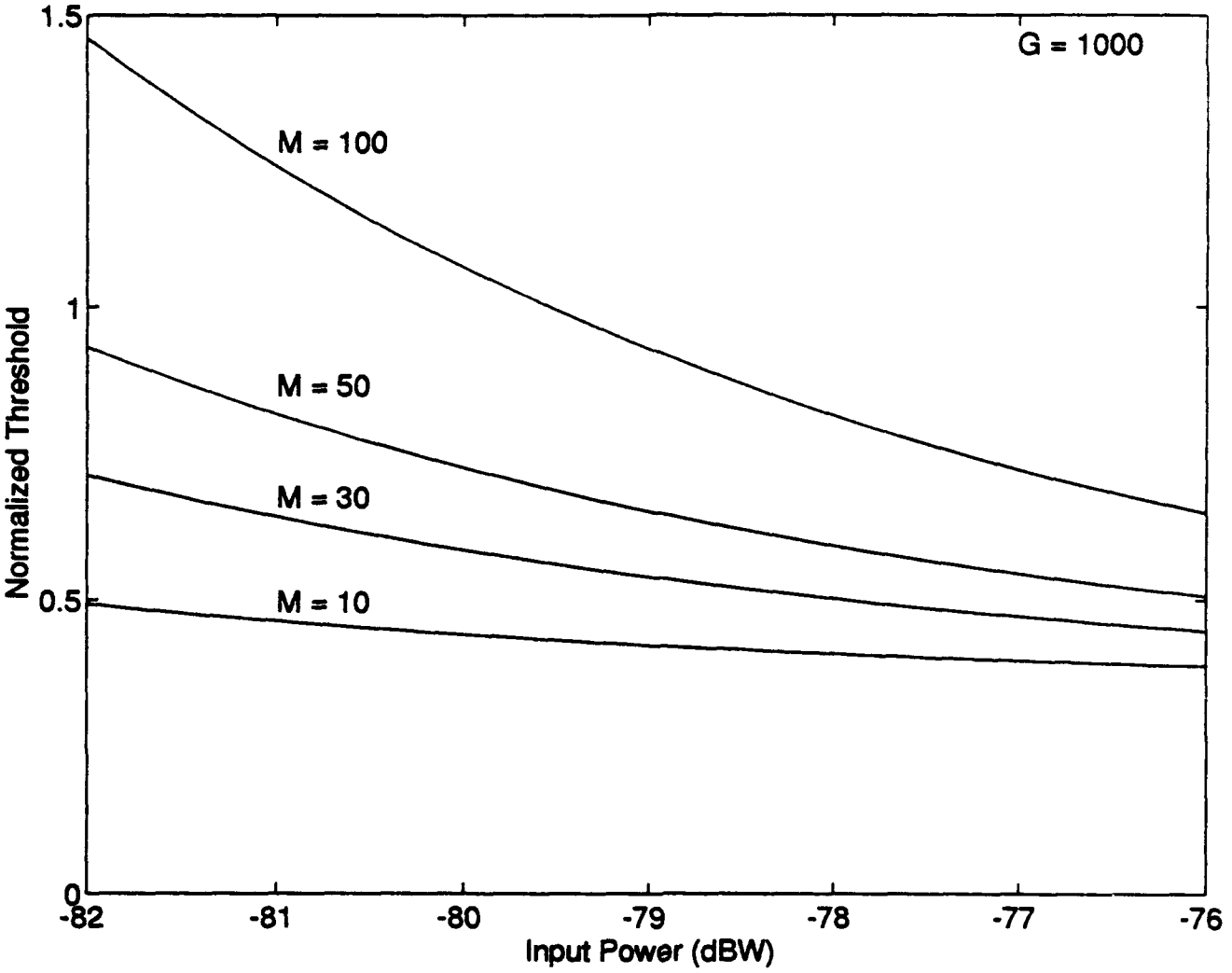

Figure 5: Optimized threshold versus input power as a function of M with $G = 1000$, postdetection thermal noise $W_0 = 10^{-22}$ A^2/Hz.

1. Mathematical Framework

Again, we adopt the complex envelope (equivalent lowpass) notation of a real OOK signal for mathematical convenience. For single channel analysis, we normally ignore the intersymbol interference (ISI) and adjacent channel interference (ACI) components. Detailed analysis including ISI and ACI components are performed in the multi-channel case. For a given transmitted bit b_i, the corresponding received signal at the input of the Fabry-Perot filter in Fig. 1 is designated as follows:

$$r_i(t) = \sqrt{GP}\, b_{0,0} p_T(t) + n_c(t) + j n_s(t) \tag{26}$$

where G is the optical amplifier gain, P is the peak power at the input of the optical amplifier, $n_c(t)$ and $n_s(t)$ are the independent in-phase and quadrature components of the zero mean AWGN representing the amplifier spontaneous emission noise (ASE) and

$$p_T = \begin{cases} 1 & 0 \le t \le T \\ 0 & \text{otherwise} \end{cases} \tag{27}$$

The Fabry-Perot filter can be characterized by the following equivalent lowpass transfer function [31, 32]

$$\begin{aligned} H(f) &= \frac{1-\rho}{1-\rho e^{-j2\pi f/FSR}} \cdot \frac{1-A-\rho}{1-\rho} \\ H(f) &= \frac{1-\rho}{1-\rho\cos\left(\frac{2\pi f}{FSR}\right) + j\rho\sin\left(\frac{2\pi f}{FSR}\right)} \cdot \frac{1-A-\rho}{1-\rho} \end{aligned} \tag{28}$$

where ρ is the power reflectivity, A is the power absorption loss ($A = 0$ for an ideal Fabry-Perot filter) and FSR is the free spectral range. For $|f| < FSR/20\pi$ and

assuming $A = 0$, we can approximate $H(f)$ as follows

$$\begin{aligned} H(f) &\approx \frac{1-\rho}{(1-\rho)+j\frac{2\pi f\rho}{FSR}} = \frac{1}{1+j\frac{2\pi f\rho}{(1-\rho)FSR}} \\ &\approx \frac{1}{1+j\frac{2\pi f}{c}}, \qquad |f| < FSR/20\pi \end{aligned} \tag{29a}$$

where

$$c = \frac{FSR(1-\rho)}{\rho} \tag{29b}$$

The free spectral range FSR can be related to the full width at half maximum (FWHM) bandwidth B and the finesse F of the Fabry-Perot filter as

$$FSR = \frac{\pi\sqrt{\rho}\,B}{1-\rho} = B \cdot F \tag{30}$$

Thus, if the signal is bandlimited to $|f| < FSR/20\pi$, we can actually use (29), but with the frequency covering the entire frequency spectral range, that is, we can truly approximate (28) with a single-pole RC filter with the following transfer function and impulse response, respectively,

$$H(f) = \frac{1}{1+j\frac{2\pi f}{c}} \tag{31}$$

$$h(t) = ce^{-ct}, \qquad t > 0 \tag{32}$$

The magnitudes of $H(f)$ of the Fabry-Perot filter in (28) and its approximated single-pole RC filter in (31) for $\rho = 0.99$, $F = 312.6$, $B = 12.16$ GHz, and $FSR = 3800$ GHz, remain identical and attenuate rapidly while the phases differ as the frequency increases [29].

The above approximation is valid for dense wavelength division multiplexing (WDM) analysis when the filter finesse F is large or equivalently the FWHM bandwidth B is small since the equivalent lowpass signal must be bandlimited to

about $|f| < FSR/20\pi$. When $|f| > FSR/20\pi$, the magnitude of $H(f)$ is very small and therefore, the effect of ACI beyond this frequency range is negligible.

a. Derivation of the Detected Signal Envelope

Since we are interested in the detected bit $b_{0,0}$ in the time interval $(0, T)$, we consider the output preamplified and filtered $S_i(t)$, given by

$$S_i(t) = S_B(t) \qquad 0 < t \leq T \tag{33}$$

where $S_B(t)$ is the desired signal, which is the convolution of the desired signal and impulse response $h(t)$ in (32), as

$$h(t) = ce^{-ct} \qquad t > 0 \tag{34}$$

$$S_B(t) = \sqrt{GP}\, b_{0,0} \int_0^t h(t-\tau)d\tau \tag{35}$$

$$S_B(t) = \sqrt{GP}\, b_{0,0}(1 - e^{-ct}) , \qquad 0 < t \leq T \tag{36}$$

The photodetector with responsivity R detects the squared envelope $R|S_i(t)|^2$. This signal plus the postdetection thermal noise current $w(t)$ are scaled by $1/TRGP$ and integrated to produce decision variable,

$$Y_i = \frac{1}{TRGP}\int_0^T R|S_i(t)|^2 dt + \frac{1}{TRGP}\int_0^T w(t)dt \tag{37}$$

$$Y_i = X_i + W \tag{38}$$

where

$$X_i = \frac{1}{TRGP}\int_0^T R|S_i(t)|^2 dt \tag{39}$$

$$W = \frac{1}{TRGP}\int_0^T w(t)dt \tag{40}$$

We model $w(t)$ as a zero mean AWGN current of spectral density of W_0. It is seen that the variance of σ_W^2 of $w(t)$ is

$$\sigma_W^2 = \frac{W_0 T}{T^2(RGP)^2} = \frac{W_0}{T(RGP)^2} \tag{41}$$

As it is described in (37), the decision variable Y_i can be easily found for zero and one bit as follows,

$$Y_0 = X_0 + W \tag{42}$$

$$Y_1 = X_1 + W \tag{43}$$

As it can be seen from above, since we ignore shot noise in this analysis, the variances of Y_1 and Y_2 are equal to each other.

$$\sigma_{Y_0}^2 = \sigma_{Y_1}^2 = \sigma_W^2 \tag{44}$$

X_i can be computed from (B.5) and found as (B.6)

$$X_i = b_{0,0}^2 \left[1 - \frac{2}{cT}(1 - e^{-ct}) + \frac{1}{2cT}(1 - e^{-2ct})\right] \tag{45}$$

Using the fact that the noise $n_c(t)$ and $n_s(t)$ are altogether independent over disjoint intervals and the random variables N_c and N_s are independent Gaussian random variables with zero mean and variance σ_i^2 computed from (B.18), we can define variance as

$$\sigma_i^2 = \frac{N_{sp} h_f (G-1)c}{4MGP} \tag{46}$$

b. Derivation of Probability Density Function of the Detected Signal Envelope

As it is described in the first section, X_i is approximately noncentral chi-squared distributed with the following probability density function (pdf) $f_{x_i}(x_i)$ [18],

$$f_{x_i}(x_i) = \frac{1}{2\sigma_i^2}\left(\frac{x_i}{\psi^2}\right)^{M-1/2} e^{-(x_i+\psi^2)/2\sigma_i^2} I_{M-1}\left(\frac{\psi\sqrt{x_i}}{\sigma_i^2}\right) \tag{47}$$

where

$$\psi^2 = b_{0,0}^2 \left[1 - \frac{2}{cT}(1 - e^{-cT}) + \frac{1}{2cT}(1 - e^{-2cT})\right] \tag{48}$$

$$b_{0,0} = \sqrt{\frac{1}{(1-r)}} \quad \text{for} \quad \text{bit one} \tag{49}$$

$$b_{0,0} = \sqrt{\frac{r}{(1+r)}} \quad \text{for} \quad \text{bit zero} \tag{50}$$

$$\sigma_i^2 \approx \frac{h_f(G-1)c}{4MGP} \tag{51}$$

In the special case where the extinction ratio $r = 0$, since $b_{0,0} = 0$ for bit zero, pdf of $f_{x_i}(x_i)$ in (47) becomes a chi-square pdf given by [18],

$$f_{x_0}(x_0) = \frac{1}{(M-1)!(2\sigma_0^2)^M} x_0^{M-1} e^{-x_0/2\sigma_0^2} \tag{52}$$

2. Bit Error Probability

For a detection threshold α, the bit error probability is conditional on the mena x_0 and x_1 and given by

$$P_b(x_0, x_1) = \frac{1}{4} erfc\left(\frac{\alpha - x_0}{\sqrt{2}\,\sigma_Y}\right) + \frac{1}{4} erfc\left(\frac{x_1 - \alpha}{\sqrt{2}\,\sigma_Y}\right) \tag{53}$$

where $erfc(\cdot)$ is defined as in (22) and $\sigma_{Y_i}^2$, $i = 0, 1$, are the variances of Y_i in (37)

$$\sigma_{Y_i}^2 = \sigma_{Y_1}^2 = \sigma_{Y_0}^2 = \sigma_W^2 \tag{54}$$

We can represent both variances as σ_Y^2, since they are equal to each other. The bit error probability is obtained by taking the expected value of $P_b(x_0, x_1)$ with respect to x_0 and x_1 using (47),

$$P_b = \frac{1}{4}\int_0^\infty erfc\left(\frac{\alpha - x_0}{\sqrt{2}\,\sigma_Y}\right) f_{x_0}(x_0)dx_0 + \frac{1}{4}\int_0^\infty erfc\left(\frac{x_1 - \alpha}{\sqrt{2}\,\sigma_Y}\right) f_{x_1}(x_1)dx_1 \tag{55}$$

The optimal threshold α that minimizes the bit error probability is the value that satisfies the following equation also given in (25)

$$\int_0^\infty erfc\left(\frac{\alpha - x_0}{\sqrt{2}\,\sigma_Y}\right) f_{x_0} dx_0 = \int_0^\infty erfc\left(\frac{x_1 - \alpha}{\sqrt{2}\,\sigma_Y}\right) f_{x_1}(x_1)dx_1 \tag{56}$$

3. Numerical Results

In this section, we present the numerical results for a single channel direct detection lightwave system employing a Fabry-Perot filter and an optical amplifier at the receiver model in Fig. 1 with the following parameters: bit rate $R_b = 500$ Mbps, optical amplifier gain $G = 100$ and 1000, photodiode responsivity $R = 0.5$, $FSR = 3800$ GHz, $c = 38.4$ GHz, $\rho = 0.99$, thermal noise spectral density $W_0 = 10^{-22}$, 10^{-23}, 10^{-24} (A^2/Hz), and $M = 10$, 13, 20, 40 where $M = T/T'$, T is the bit duration $(1/R_b)$ and T' is the time constant of the optical bandpass filter. Since bit rate $R_b = 500$ Mbps, bit duration T is 2 ns. If we chop the impulse response of the filter at 0.05 ns, 0.1 ns, 0.15 ns, and 0.2 ns, M has the values of 40, 20, 13, 10, respectively. Figures 6, 7, and 8 show the bit error probability P_b versus peak input power P (dBW) as a function of M for the thermal noise spectral density $W_0 = 10^{-22}$, 10^{-23}, 10^{-24} A^2/Hz with $G = 100$. As M decreases, it is obvious that more input power is required to achieve $P_b = 10^{-15}$ as compared to finite-time integrator. In the case where finite-time integrator is employed as M decreases, less input power is required because the noise variance given in (16),

$$\sigma^2 = \frac{N_{sp}hf(G-1)}{2GPT}$$

is independent of M and even if T' is varied, it has constant T. Therefore, varying M does not effect the noise variance but it effects the signal power. For the Fabry-Perot filter, the variance given in (46),

$$\sigma_i^2 = \frac{N_{sp}hf(G-1)c}{4MGP}$$

depends on the M value, and as T' is varied, M varies accordingly ($M = T/T'$). So, as M decreases, noise variance gets larger and more power is required to achieve $P_b = 10^{-15}$. As it can be easily seen from these figures, the role of T' is more

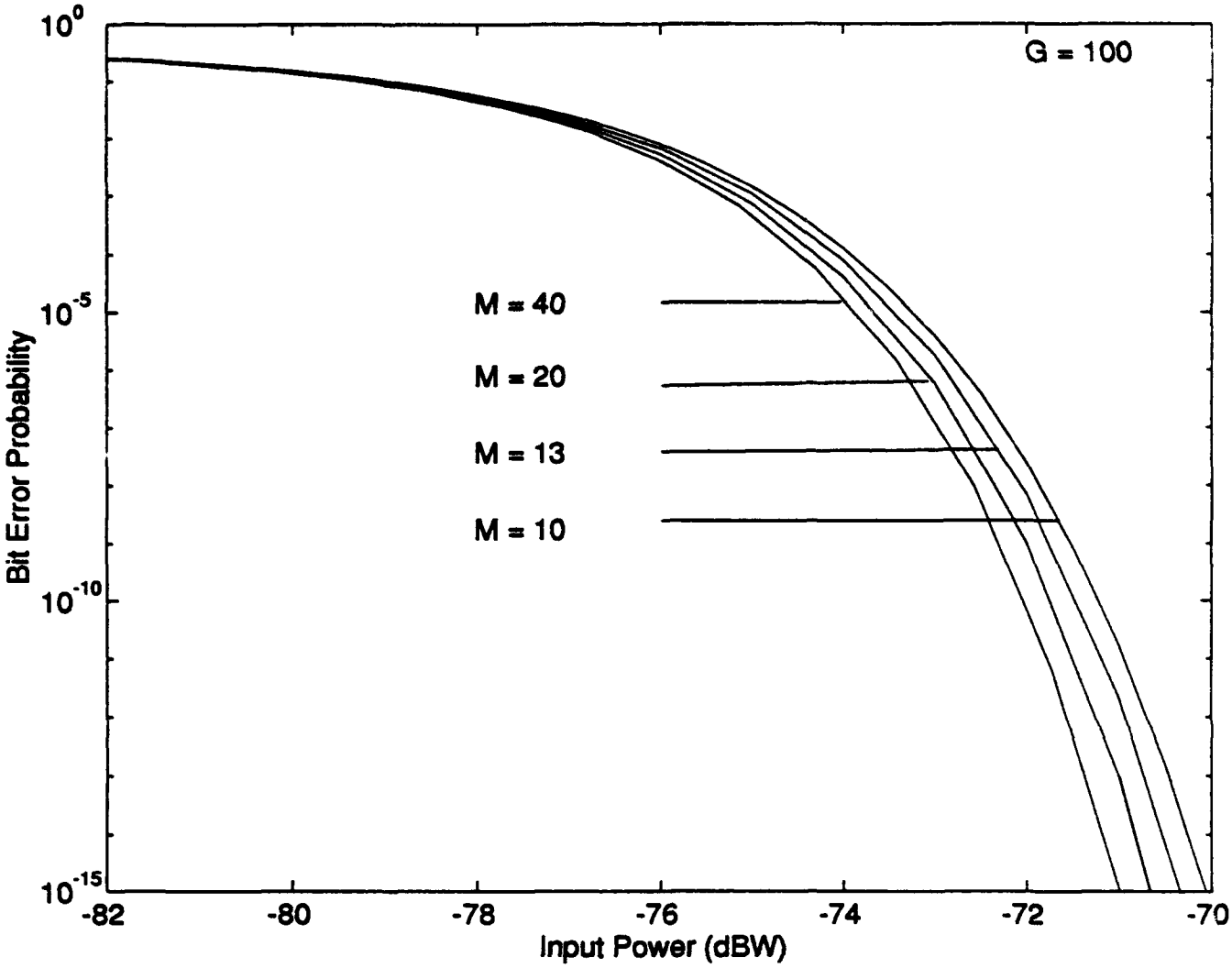

Figure 6: Bit error probability versus input power as a function of M with $G = 100$, $W_0 = 10^{-22}$ A^2/Hz (Fabry-Perot filter).

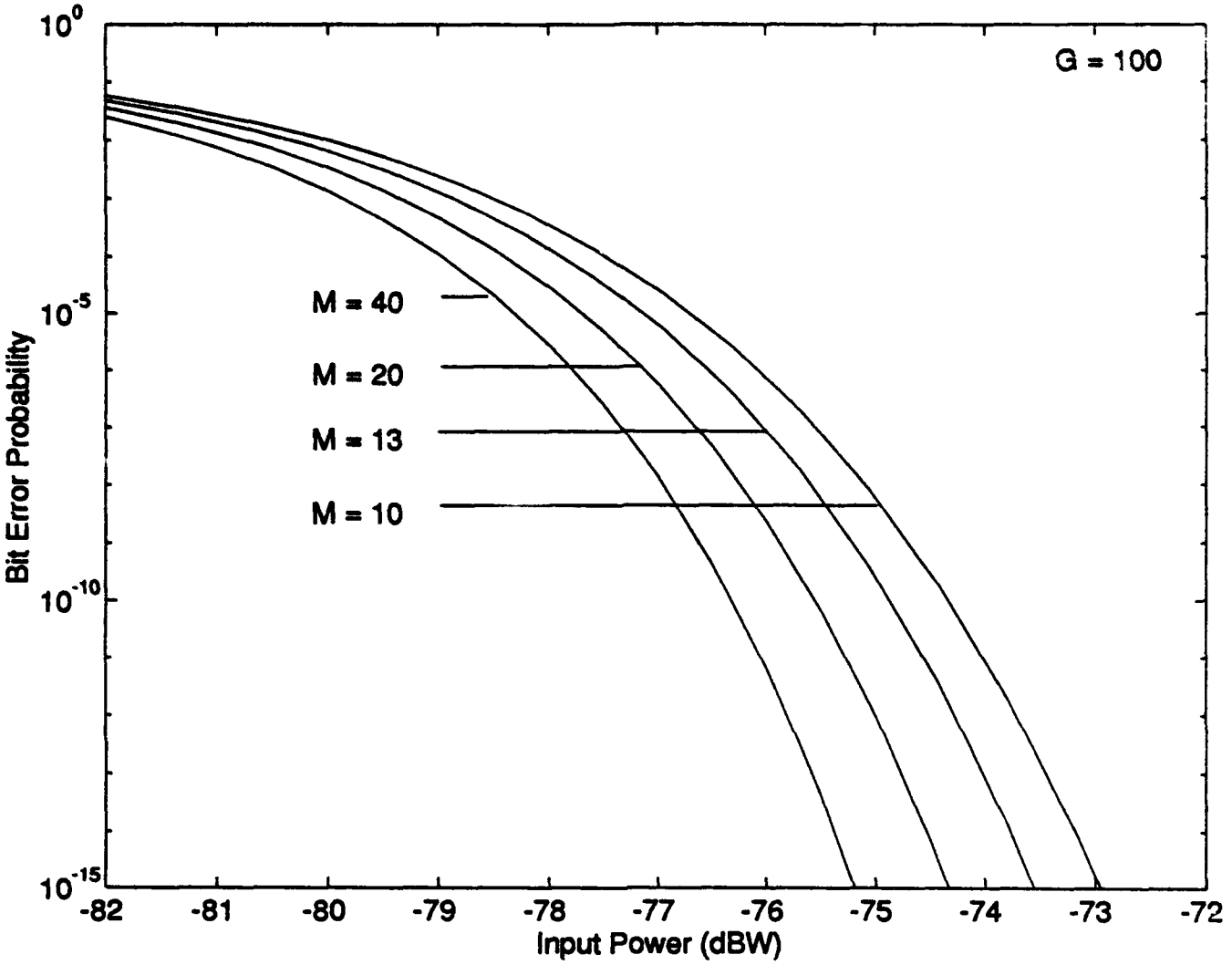

Figure 7: Bit error probability versus input power as a function of M with $G = 100$, $W_0 = 10^{-23}$ A^2/Hz (Fabry-Perot filter).

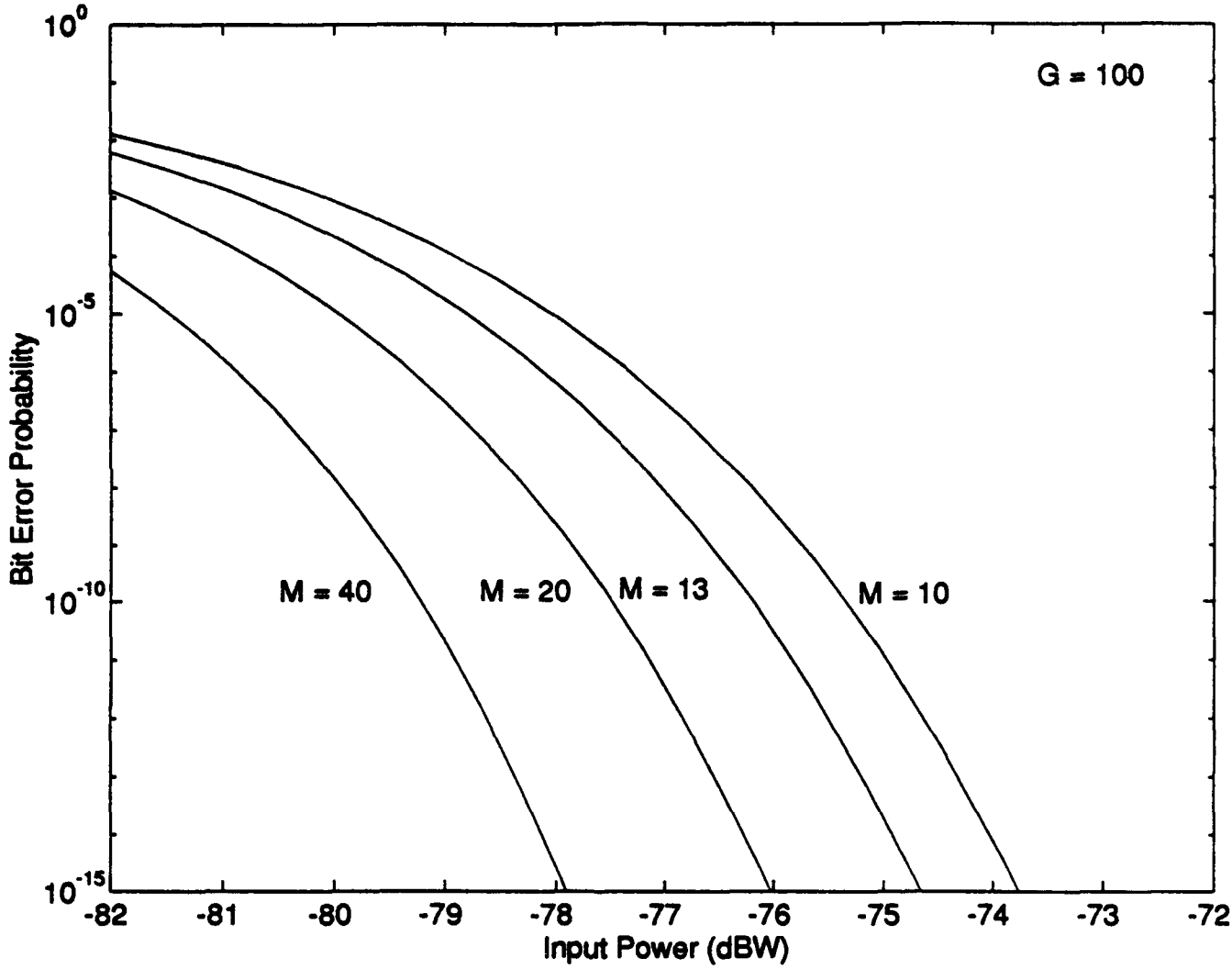

Figure 8: Bit error probability versus input power as a function of M with $G = 100$, $W_0 = 10^{-24}$ A^2/Hz (Fabry-Perot filter).

significant for smaller thermal noise values. This is more pronounced with a high gain amplifier ($G = 1000$) as can be seen in Tables 1 and 2 and Figs. 9, 10, and 11. Detailed comparison is as follows:

Table 1: Comparison between $M = 10$ and $M = 40$ with $G = 100$ (see Figs. 6, 7, and 8).

W_0 (A^2/Hz)	$M = 40$ ($T' = 0.05$ ns) (dBW)	$M = 10$ ($T' = 0.2$ ns) (dBW)	Difference (dBW)
10^{-22}	-71.0	-70.0	1.0
10^{-23}	-75.2	-73.0	2.2
10^{-24}	-78.9	-73.8	5.1

Table 2: Comparison between $M = 10$ and $M = 40$ with $G = 1000$ (see Figs. 9, 10, and 11).

W_0 (A^2/Hz)	$M = 40$ ($T' = 0.05$ ns) (dBW)	$M = 10$ ($T' = 0.2$ ns) (dBW)	Difference (dBW)
10^{-22}	-77.9 dB	-73.8 dB	4.1 dB
10^{-23}	-78.7 dB	-73.9 dB	4.8 dB
10^{-24}	-78.8 dB	-73.9 dB	4.9 dB

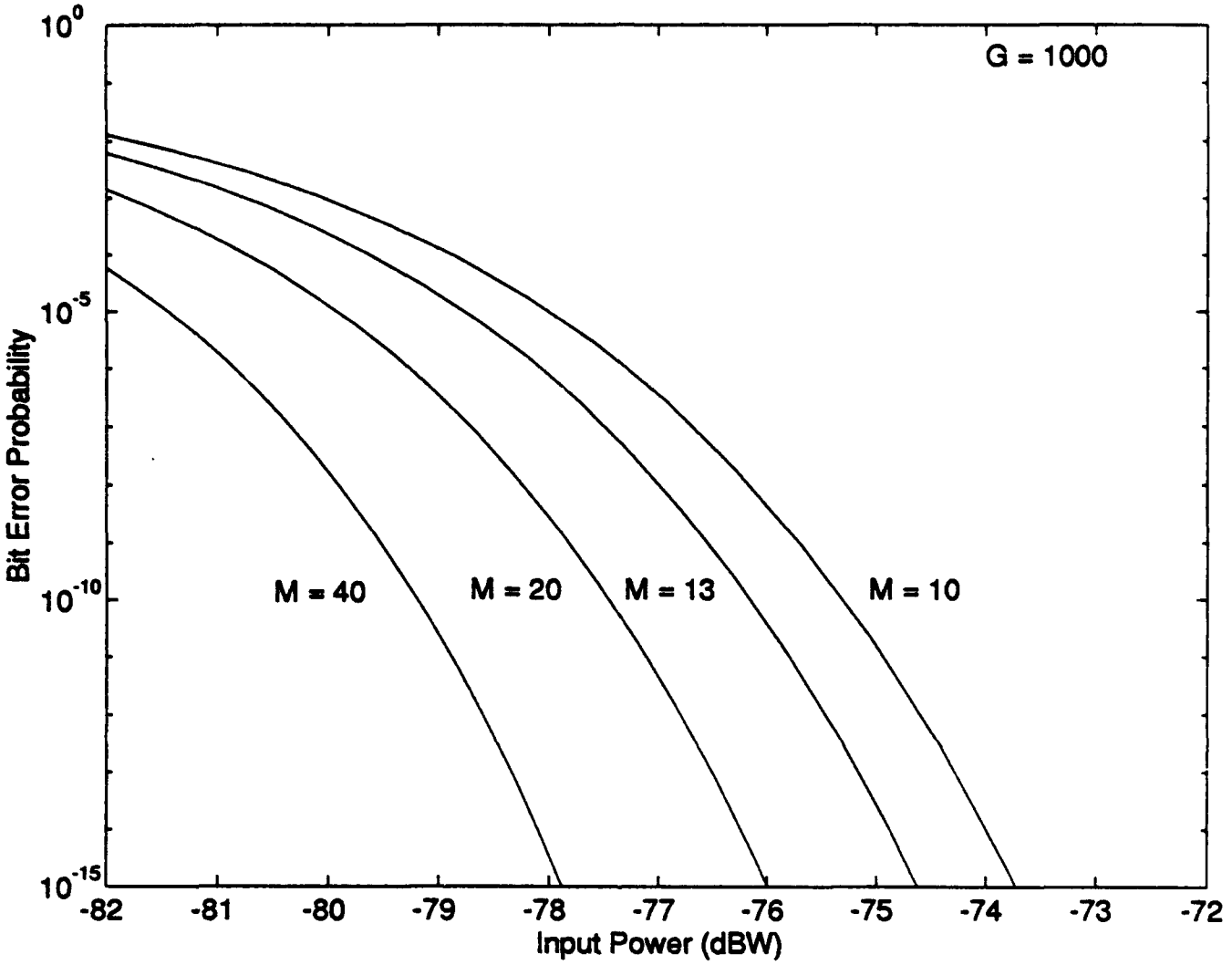

Figure 9: Bit error probability versus input power as a function of M with $G = 1000$, $W_0 = 10^{-22}$ A^2/Hz (Fabry-Perot filter).

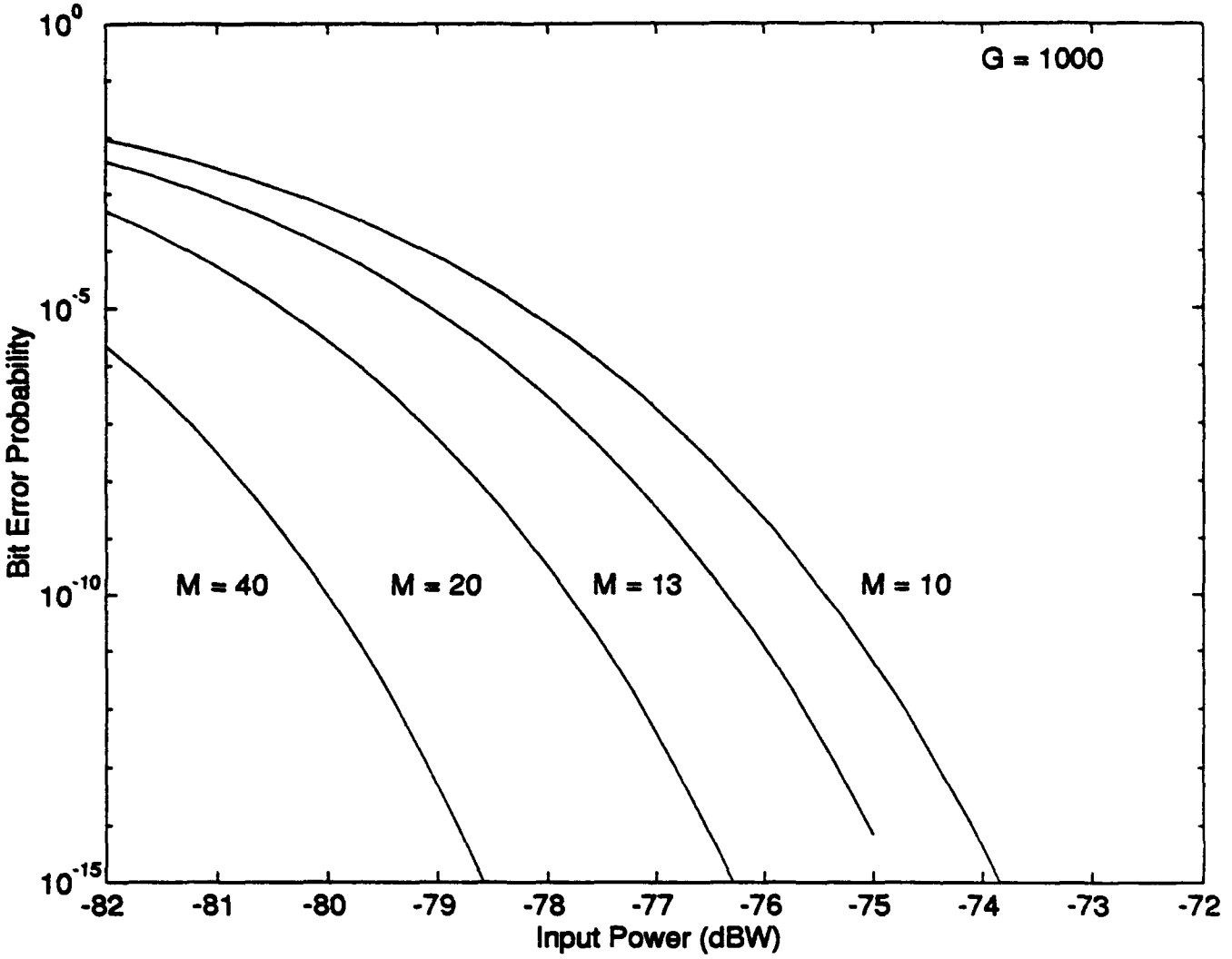

Figure 10: Bit error probability versus input power as a function of M with $G = 1000$, $W_0 = 10^{-23}$ A^2/Hz (Fabry-Perot filter).

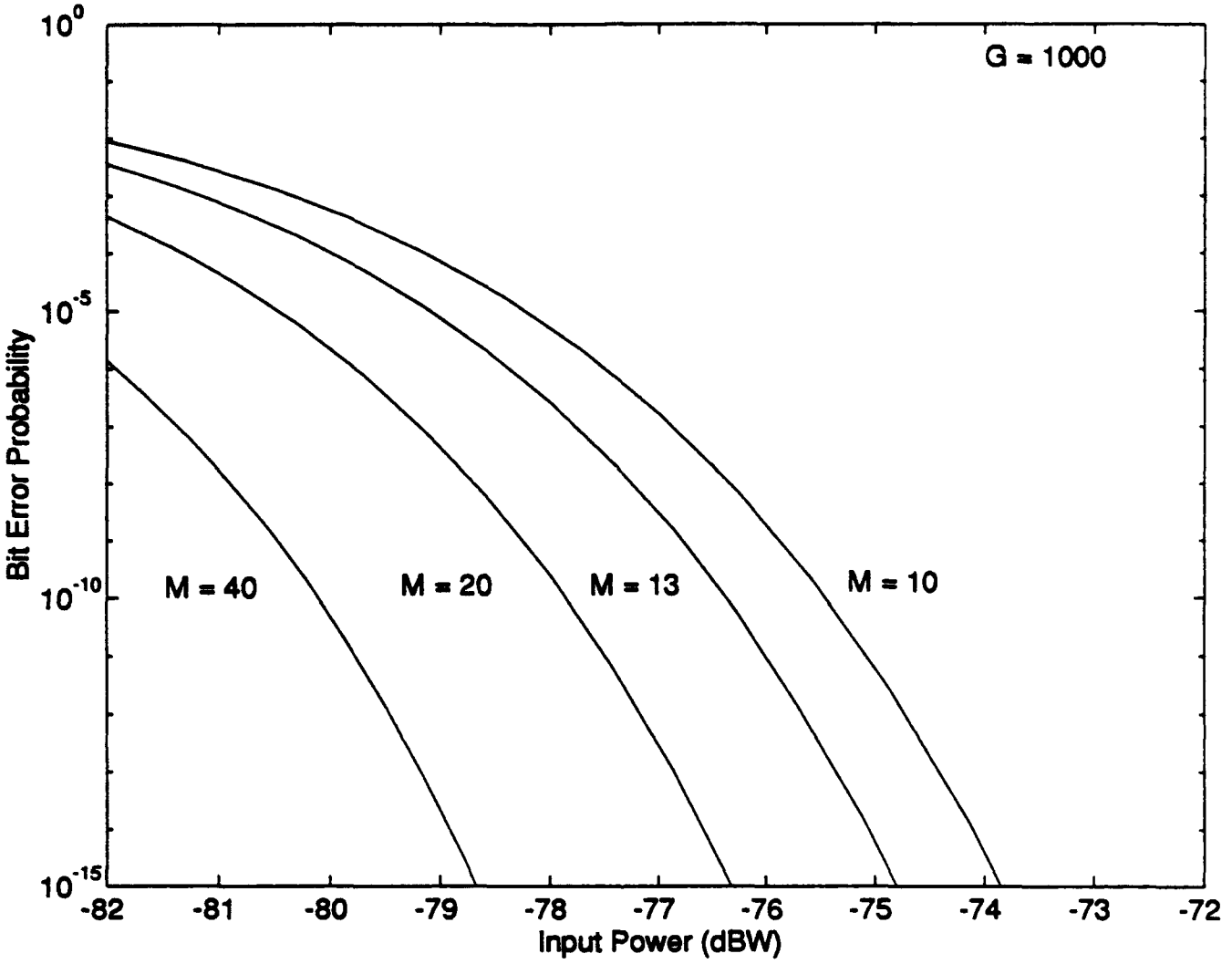

Figure 11: Bit error probability versus input power as a function of M with $G = 1000$, $W_0 = 10^{-24}$ A^2/Hz (Fabry-Perot filter).

When we compare the finite-time integrator and Fabry-Perot filter with each other, Table 3 shows that the finite-time integrator has better performance than the Fabry-Perot filter for larger T'. This improvement of the finite-time integrator over the Fabry-Perot filter gets more significant with high gain amplifiers and lower thermal noise values as displayed in Table 4. Performance margins decrease with increasing thermal noise values.

Figures 14 and 15 show that the Fabry-Perot filter has better performance than finite-time integrators with a low amplifier gain ($G = 100$) for low thermal noise values ($W_0 = 10^{-23}$ A^2/Hz, 10^{-24} A^2/Hz) and both have the same performance for a higher thermal noise value of $W_0 = 10^{-22}$ A^2/Hz with smaller T', which implies a higher values of M due to the relation of M and T' ($M = T/T'$) for a constant bit rate. This improvement of the Fabry-Perot filter over the finite-time integrator is more pronounced with a high gain amplifier ($G = 1000$) as shown in Figs. 16 and 17 and tabulated in Tables 5 and 6.

As a result, the choice of T' and consequently, the value of M plays a great role for the systems employing the Fabry-Perot filter and the high gain amplifier when the postdetection thermal noise is small. The systems employing finite-time integrators and high gain amplifiers have better performance than those employing the Fabry-Perot filter when T' (time constant of the filter) is large and thermal noise is small. The systems with the Fabry-Perot filter and the high gain amplifier have better performance than the finite-time integrator when T' is small and thermal noise is low.

Table 3: Comparison between FTI and FP for $G = 100$, $r = 0$, and $M = 10$ (see Figs. 6, 7, 8, and 12).

W_0 (A^2/Hz)	FTI (Input Power) (dBW)	Fabry-Perot (Input Power) (dBW)	Remarks Improvement of FTI
10^{-22}	−71.1	−70.0	1.1
10^{-23}	−75.3	−73.0	2.3
10^{-24}	−78.5	−73.8	4.7

Table 4: Comparison between FTI and FP for $G = 1000$, $r = 0$, and $M = 10$ (see Figs. 9, 10, 11, and 13).

W_0 (A^2/Hz)	FTI (Input Power) (dBW)	Fabry-Perot (Input Power) (dBW)	Remarks Improvement of FTI
10^{-22}	−78.5	−73.8	4.7
10^{-23}	−79.6	−73.9	5.7
10^{-24}	−79.8	−73.9	5.9

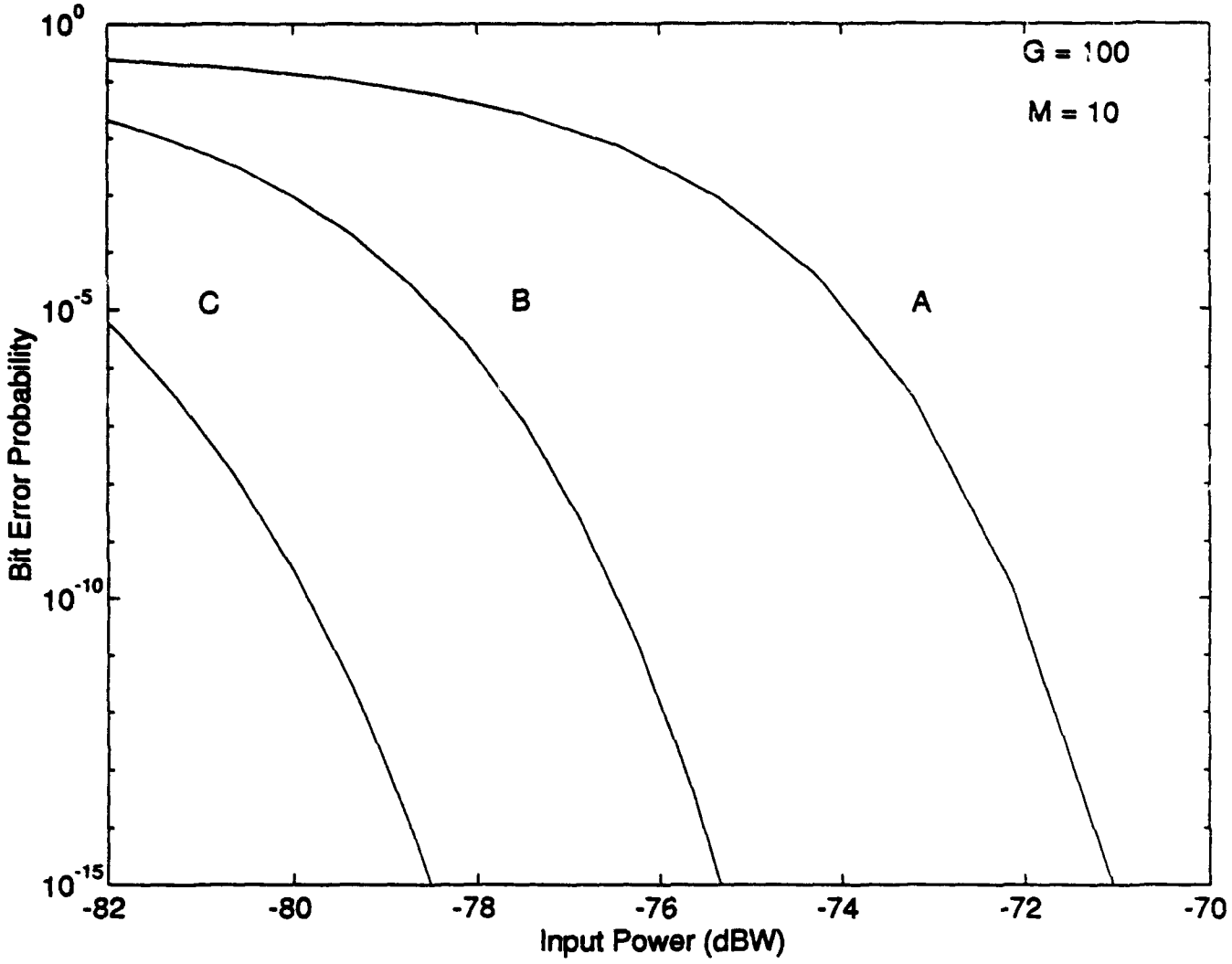

Figure 12: Bit error probability versus input power as a function of postdetection thermal noise W_0 with optical amplifier gain $G = 100$, extinction ration $r = 0$, $M = 10$. A: 10^{-22} A^2/Hz, B: 10^{-23} A^2/Hz, C: 10^{-24} A^2/Hz (finite-time integrator).

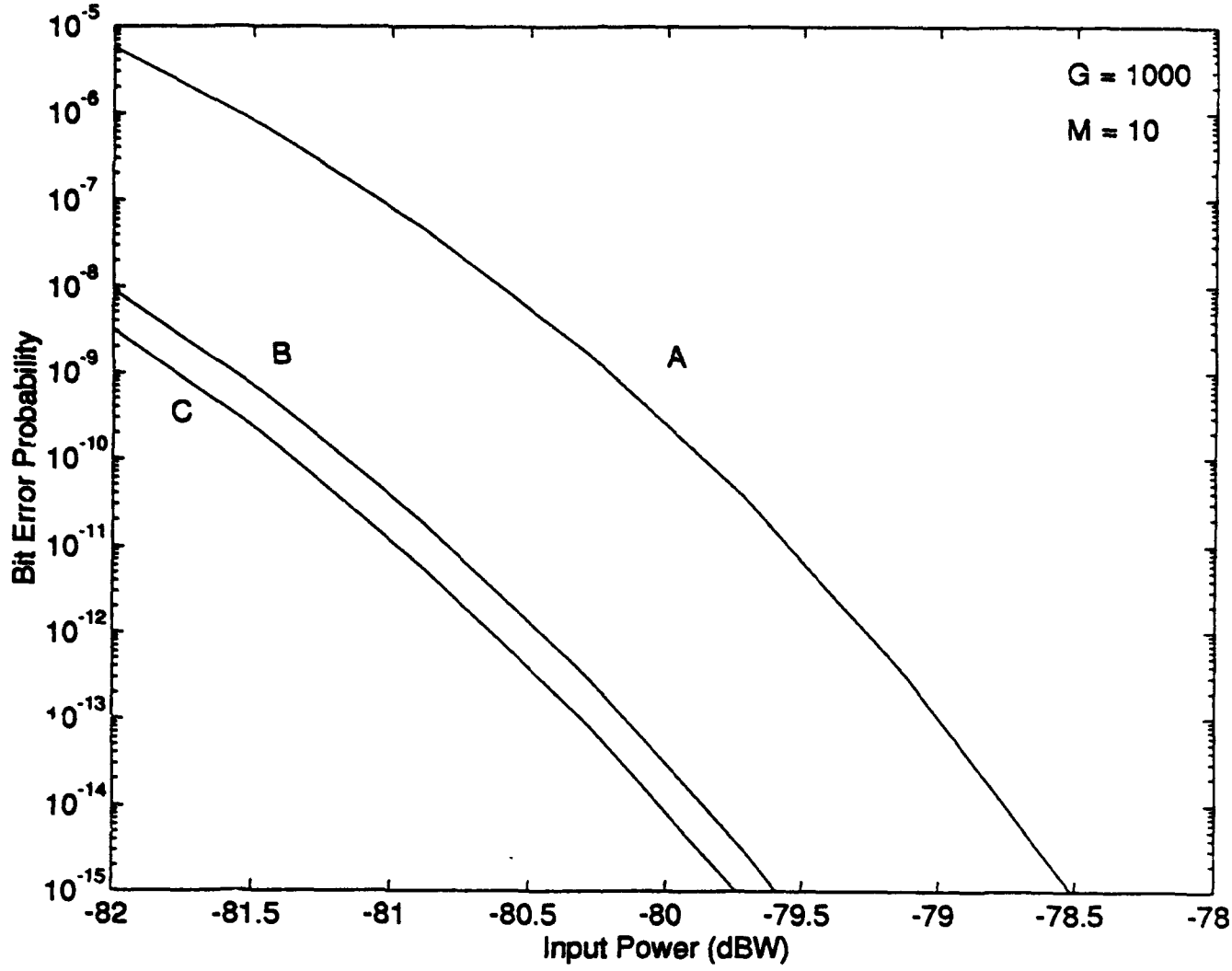

Figure 13: Bit error probability versus input power as a function of postdetection thermal noise W_0 with optical amplifier gain $G = 1000$, extinction ration $r = 0$, $M = 10$. A: 10^{-22} A^2/Hz, B: 10^{-23} A^2/Hz, C: 10^{-24} A^2/Hz (finite-time integrator).

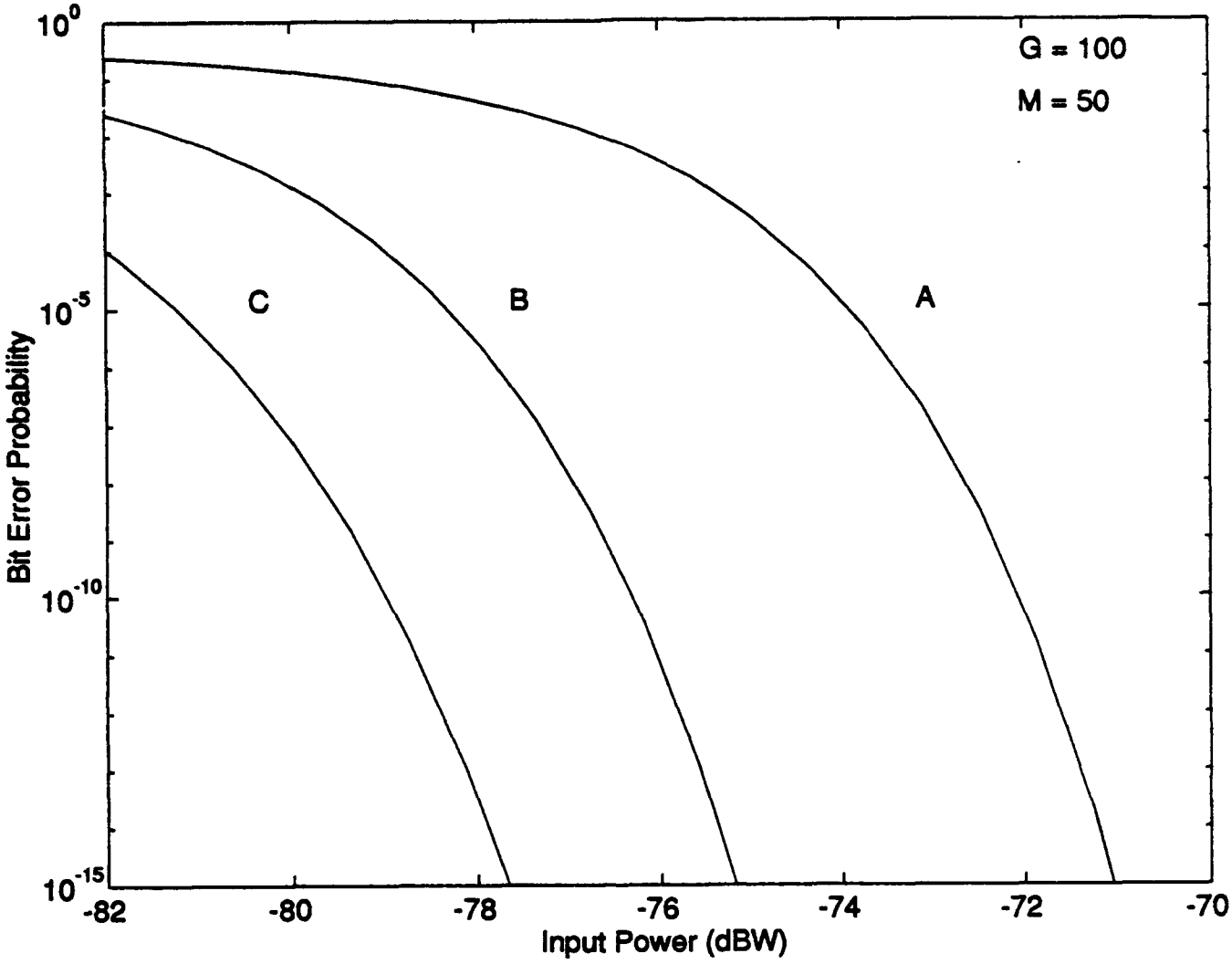

Figure 14: Bit error probability versus input power as a function of postdetection thermal noise W_0 with optical amplifier gain $G = 100$, extinction ration $r = 0$, $M = 50$. A: 10^{-22} A^2/Hz, B: 10^{-23} A^2/Hz, C: 10^{-24} A^2/Hz (finite-time integrator).

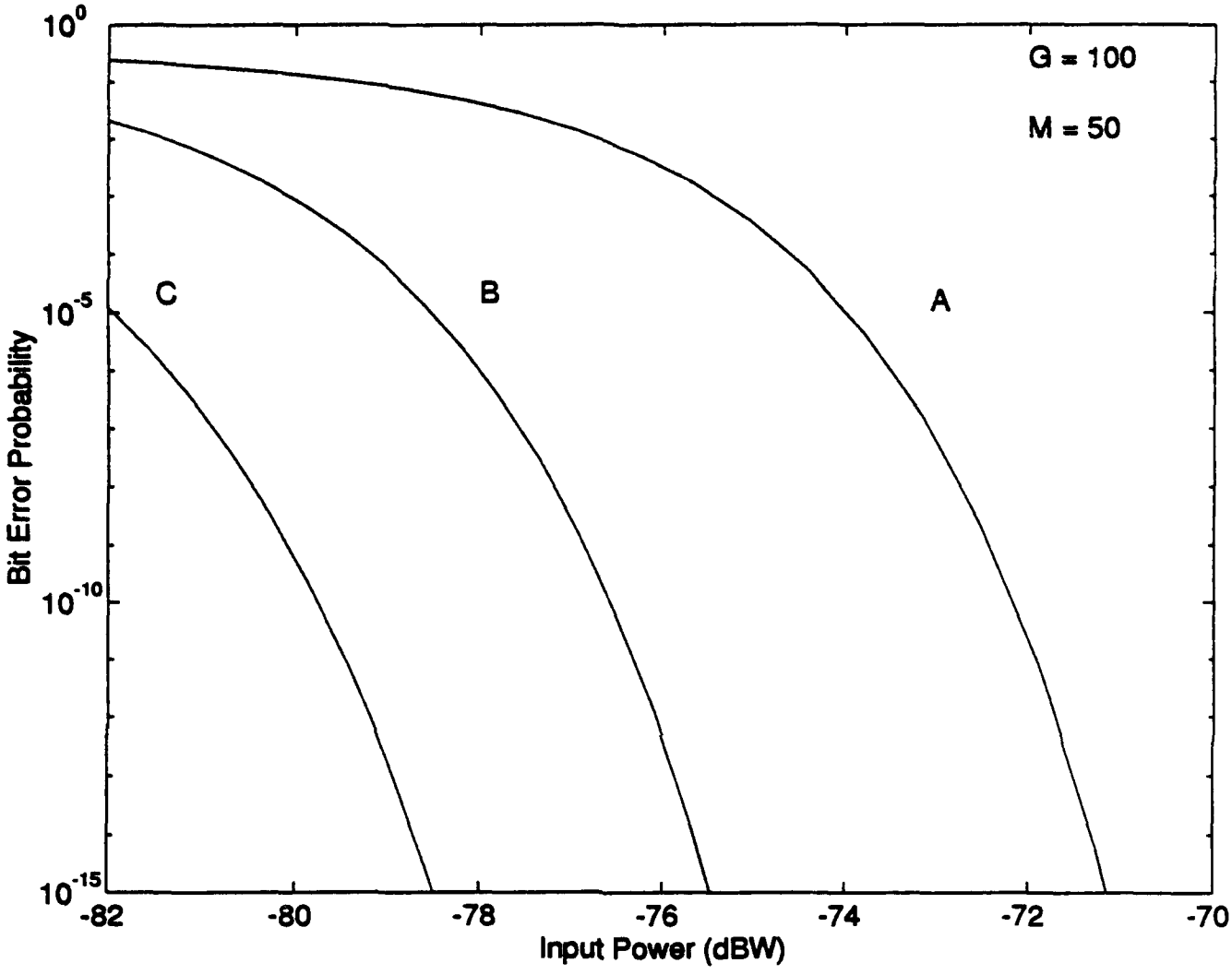

Figure 15: Bit error probability versus input power as a function of postdetection thermal noise W_0 with optical amplifier gain $G = 100$, extinction ration $r = 0$, $M = 50$. A: 10^{-22} A^2/Hz, B: 10^{-23} A^2/Hz, C: 10^{-24} A^2/Hz (Fabry-Perot filter).

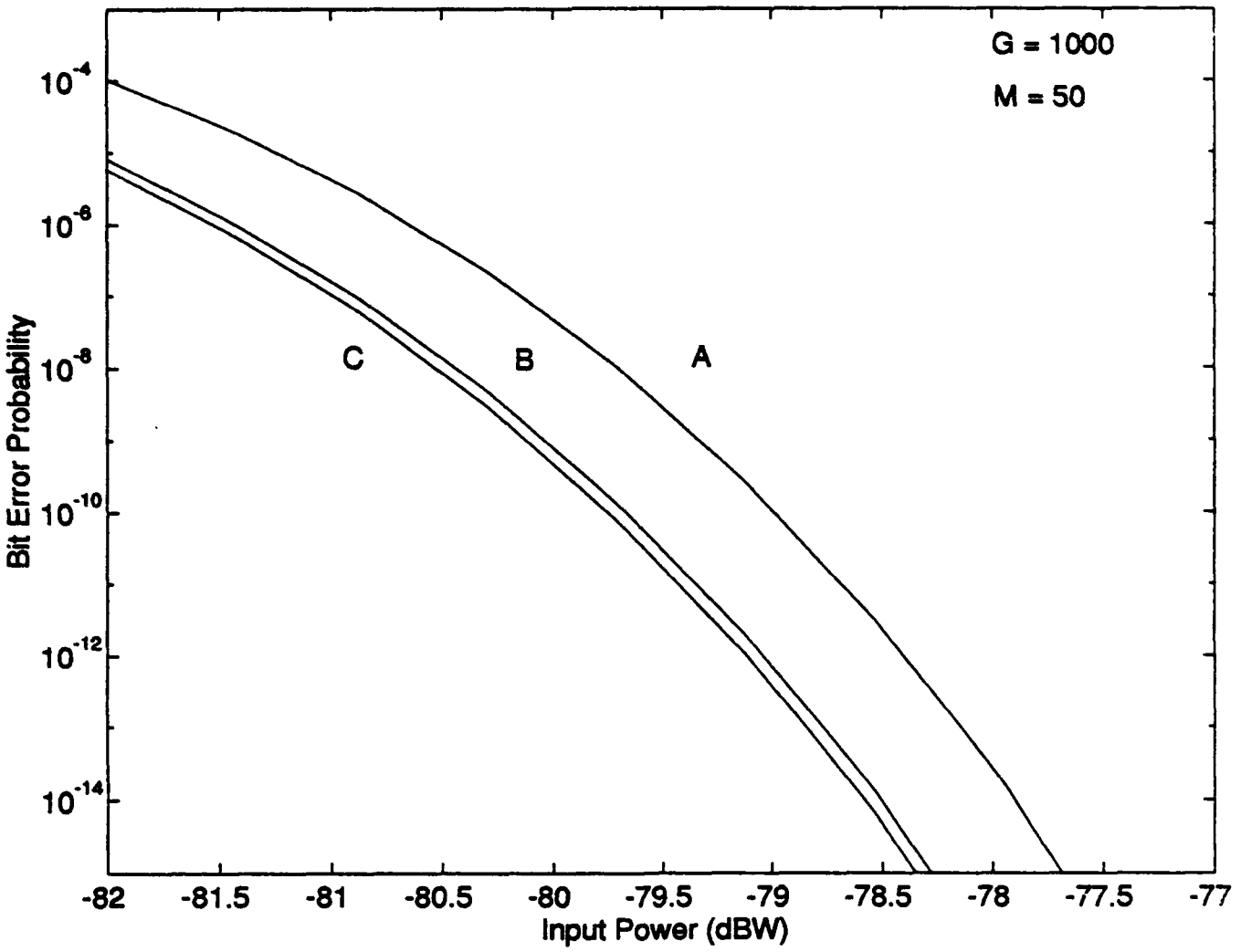

Figure 16: Bit error probability versus input power as a function of postdetection thermal noise W_0 with optical amplifier gain $G = 1000$, extinction ration $r = 0$, $M = 50$. A: 10^{-22} A^2/Hz, B: 10^{-23} A^2/Hz, C: 10^{-24} A^2/Hz (finite-time integrator).

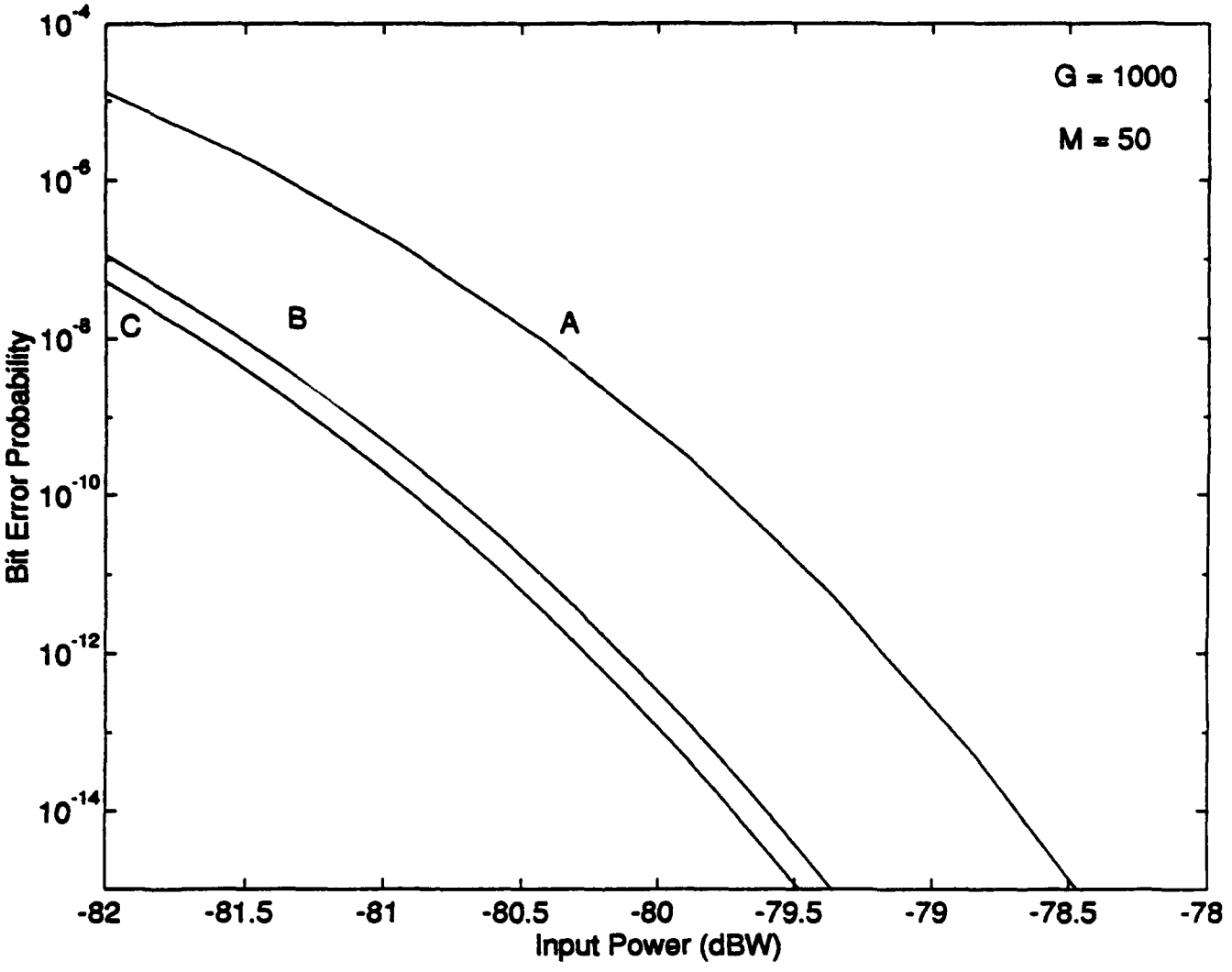

Figure 17: Bit error probability versus input power as a function of postdetection thermal noise W_0 with optical amplifier gain $G = 1000$, extinction ration $r = 0$, $M = 50$. A: 10^{-22} A^2/Hz, B: 10^{-23} A^2/Hz, C: 10^{-24} A^2/Hz (Fabry-Perot filter).

Table 5: Comparison between FTI and FP for $G = 100$, $r = 0$, and $M = 50$ (see Figs. 14 and 15).

W_0 (A^2/Hz)	FTI (Input Power) (dBW)	Fabry-Perot (Input Power) (dBW)	Remarks Improvement of Fabry-Perot is
10^{-22}	−71.1	−71.1	0
10^{-23}	−75.2	−75.4	0.2
10^{-24}	−77.8	−78.5	0.7

Table 6: Comparison between FTI and FP for $G = 1000$, $r = 0$, and $M = 50$ (see Figs. 16 and 17).

W_0 (A^2/Hz)	FTI (Input Power) (dBW)	Fabry-Perot (Input Power) (dBW)	Remarks Improvement of Fabry-Perot is
10^{-22}	−77.7	−78.5	0.8
10^{-23}	−78.35	−79.4	1.05
10^{-24}	−78.4	−79.5	1.1

C. FABRY-PEROT FILTER FOR MULTI-CHANNEL

In the previous section, we considered only the desired bit signal rather than the ISI and ACI components since we dealt with a single channel. In this section, we take into account the ISI and ACI components and our analysis focuses on the multi-channel.

1. Mathematical Framework

For convenience, we designate channel 0 as the desired channel and channel k as the adjacent channel where $k = -M/2, \cdots, -1, 1, \cdots, M/2$ and M is an even integer. We consider the equivalent lowpass (complex envelope) data signal in channel 0 and channel k as follows,

$$b_0(t) = \sum_{i=-b_0}^{0} b_{0,i} p_T(t - iT) \tag{57}$$

$$b_k(t) = \sum_{i=-L}^{0} b_{k,\ell} e^{jw_k t} p_T(t - \ell T) \tag{58}$$

where T is the bit duration, $b_{0,i} \epsilon \{0, 1\}$ is the bit in channel 0 in the time interval $(iT, (i+1)T)$, $b_{k,\ell} \epsilon \{0, e^{j\phi}\}$ is the ℓ^{th} bit in channel k in the time interval $(\ell T, (\ell+1)T)$, ϕ_k is a phase offset between channel 0 and channel k, which is assumed to be uniformly distributed in $(0, 2\pi)$ radians, and w_k is the frequency spacing between channel 0 and channel k in radians.

The function $p_T(t - iT)$ is defined as

$$p_T(t - iT) = \begin{cases} 1 & iT < t < (i+1)T \\ 0 & \text{otherwise} \end{cases} \tag{59}$$

The non-negative integers L_0 and L in (57) and (58) represent the number of bits in channel 0 and k, respectively, that precede the detected bits $b_{0,0}$. The received

WDM equivalent lowpass signal at the input of the Fabry-Perot filter is given by,

$$r(t) = \sqrt{GP}\, b_0(t) + \sum_{\substack{k=M/2 \\ k\neq 0}}^{M/2} \sqrt{GP}\, b_k(t) \tag{60}$$

where P is the received optical power and G is the gain of the preamplifier.

As we discussed in the previous section, the impulse response of the Fabry-Perot filter is approximated by a single-pole RC filter of which the impulse response is given in (32) as,

$$h(t) = ce^{-ct}, \qquad t > 0 \tag{61}$$

a. Derivation of the Detected Signal Envelope

The output preamplified and filtered signal $S_i(t)$ is given as,

$$S_i(t) = S_B(t) + S_{ISI}(t) + S_{ACI}(t), \qquad 0 < t \leq T \tag{62}$$

where $S_B(t)$ is the desired bit signal, $S_{ISI}(t)$ is the intersymbol interference signal, and $S_{ACI}(t)$ is the adjacent channel interference signal. These signals are evaluated to obtain output filtered signals by using (60) and (61),

$$\begin{aligned} S_B(t) &= \sqrt{GP}\, b_{0,0} \int_0^t h(t-\tau)d\tau \\ &= \sqrt{GP}\, b_{0,0}(1 - e^{-ct}), \qquad 0 < t \leq T \end{aligned} \tag{63}$$

$$\begin{aligned} S_{ISI}(t) &= \sqrt{GP} \sum_{i=L_0}^{-\ell} b_{0,i} \int_{iT}^{(i+1)T} h(t-\tau)d\tau \\ &= \sqrt{GP}e^{-ct} \sum_{i=L_0}^{-1} b_{0,i} \left(e^{(i+1)cT} - e^{icT}\right), \qquad 0 < t \leq T \end{aligned} \tag{64}$$

$$S_{ACI}(t) = \sqrt{GP} \sum_{\substack{k=-M/2 \\ k\neq 0}}^{M/2} \left\{ \left[\sum_{\ell=-L}^{-1} b_{k,\ell} \int_{\ell T}^{\ell+1} h(t-\tau) e^{jw_k\tau} d\tau \right] \right.$$

$$\left. + b_{k,0} \int_0^t h(t-\tau) e^{jw_k\tau} d\tau \right\}$$

$$= \sqrt{GP}\, e^{-ct} \sum_{\substack{k=-M/2 \\ k\neq 0}}^{M/2} \frac{1}{c+jw_k} \left\{ \left[\sum_{\ell=-L}^{-1} b_{k,\ell} \left(e^{(c+jw_k)(\ell+1)T} - e^{(c+jw_k)\ell T} \right) \right] \right.$$

$$\left. + b_{k,0} \left(e^{(c+jw_k)} - 1 \right) \right\}, \qquad 0 < t \leq T \tag{65}$$

The Fabry-Perot filtered output $S_i(t)$ is detected by the photodetector. The detected current signal is amplified by a low noise amplifier (LAN) that contributes a postdetection thermal noise $w(t)$ with spectral density N_0 (A^2/Hz). The decision variable at the output of the integration is compared to a threshold α to determine whether bit zero or bit one is present. The decision variable Y is given by (37) as,

$$Y = X_i + W \tag{66}$$

where

$$X_i = \frac{1}{TRGP} \int_0^T R|S_i(t)|^2 dt \tag{67}$$

$$W = \frac{1}{TRGP} \int_0^T W(t) dt \tag{68}$$

We obtain the signal component X_i by substituting (62), (63), (64), and (65) into (67) as a function of cT and w_kT, which represents the impact of ISI and ACI, respectively. X_i can be obtained from (C.19) for the worst case analysis as follows [29],

$$X_i = \frac{1}{TRGP} \left[TRGP \left(b_{0,0}^2 \left[1 - \frac{2}{cT}(1 - e^{-cT}) + \frac{1}{2cT}(1 - e^{-2cT}) \right] \right. \right.$$

$$+b_-^2\left[\frac{1}{2cT}(1-e^{-2cT})\right]+b_{0,0}b_-\left[\frac{1}{cT}(1-2e^{-cT}+e^{-2cT})\right]$$
$$+\left[|b|^2+\frac{2}{cT}(1-e^{-cT})Re\{b\}(b_--b_{0,0})\right.$$
$$\left.\cdot\sum_{\substack{k=-M/2\\k\neq 0}}^{M/2}\frac{1}{1+\left(\frac{w_k}{c}\right)^2}\right)\Bigg] \qquad (69a)$$

where

$$b_{0,0}=0 \quad \text{for bit zero} \qquad b_{0,0}=1 \quad \text{for bit one,}$$
$$b_-=1 \quad \text{for bit zero} \qquad b_-=0 \quad \text{for bit one,}$$
$$b=1 \quad \text{for bit zero} \qquad b=0 \quad \text{for bit one}$$

in the worst case analysis.

For the exact case analysis, X_i, which is derived in [29] for the case without the optical amplifier, can be modified for our case as follows,

$$X_i = \frac{1}{TRGP}\int_0^T R|S_i(t)|^2dt$$
$$X_i = \frac{1}{TRGP}\left[TRGPb_{0,0}^2\left[1-\frac{2}{cT}\left(1-e^{-cT}\right)+\frac{1}{2cT}\left(1-e^{-2cT}\right)\right]\right.$$
$$+TRGP\frac{1}{2cT}\left(1-e^{-2cT}\right)\left[\sum_{i=L_0}^{-1}b_{0,i}\left(e^{(i+1)cT}-e^{icT}\right)\right]^2$$
$$+TRGP\frac{1}{2cT}\left(1-e^{-2cT}\right)\left|\sum_{\substack{k=-M/2\\k\neq 0}}^{M/2}\sum_{\ell=-L}^{-1}\frac{b_{k,\ell}}{\ell+jw_kT/cT}\right.$$
$$\left.\left(e^{(cT+jw_kT)(\ell+1)}e^{(cT+jw_kT)\ell}\right)\right|^2$$
$$\left.+TRGP\frac{1}{cT}\sum_{\substack{k=-M/2\\k\neq 0}}^{M/2}\sum_{\substack{m=-M/2\\m\neq 0}}^{M/2}\frac{b_{k,0}b_{m,0}^*}{(1+jw_kT/cT)(1-jw_mT/cT)}\right.$$

$$\left\{\left[cT+\frac{e^{-(cT-jw_kT)}-1}{1-jw_kT/cT}+\frac{e^{-(cT+jw_mT)}-1}{1+jw_nT/cT}+\frac{1}{2}\left(1-e^{-2cT}\right)\right]\right\}$$

$$+2GPT\frac{1}{cT}R_c\Bigg\{\sum_{\substack{k=-M/2\\k\neq 0}}^{M/2}\sum_{\substack{m=-M/2\\m\neq 0}}^{M/2}\sum_{\ell=-L}^{-1}\frac{b_{k,\ell}b^*_{m,0}}{(1+jw_kT/cT)(1-jw_mT/cT)}$$

$$\left(e^{(cT+jw_kT)(\ell+1)}-e^{(cT+jw_kT)\ell}\right)\left[\frac{1-e^{-(cT+jw_mT)}}{1+jw_nT/cT}-\frac{1}{2}\left(1-e^{-2cT}\right)\right]\Bigg\}$$

$$+GPTb_{0,0}\frac{1}{cT}\left(1+e^{-2cT}-2e^{-cT}\right)\sum_{i=-L_0}^{-1}b_{0,i}\left(e^{(i+1)cT}-e^{icT}\right)$$

$$+GPTb_{0,0}\frac{1}{cT}R_e\Bigg\{\left(1+e^{-2cT}-2e^{-cT}\right)$$

$$\sum_{\substack{k=-M/2\\k\neq 0}}^{M/2}\sum_{\ell=-L}^{-1}\frac{b_{k,\ell}}{1+jw_kT/cT}\left(e^{(cT|jw_kT)(\ell+1)}-e^{(cT+jw_kT)\ell}\right)$$

$$+2\sum_{\substack{k=-M/2\\k\neq 0}}^{M/2}\frac{b_{k,0}}{1+jw_kT/cT}\Bigg(\frac{e^{jw_kT}-1}{jw_kT/cT}+e^{-cT}-\frac{1}{2}-\frac{1}{2}e^{-2cT}$$

$$+\frac{e^{-(cT-jw_kT)}-1}{1-jw_kT/cT}\Bigg)\Bigg\}+\frac{GPT}{cT}\sum_{i=-L_0}^{-1}b_{0,i}\left(e^{(i+1)cT}-e^{icT}\right)$$

$$R_e\Bigg\{\sum_{\substack{k=-M/2\\k\neq 0}}^{M/2}\sum_{\ell=-L}^{-1}\frac{b_{k,\ell}}{1+jw_kT/cT}\left(1-e^{-2cT}\right)$$

$$\left(e^{(cT+jw_kT)(\ell+1)}-e^{(cT+jw_kT)\ell}\right)$$

$$+\sum_{\substack{k=-M/2\\k\neq 0}}^{M/2}\frac{b_{k,0}}{1+jw_kT/cT}\left(\frac{2(1-e^{-(cT-jw_kT)})}{1-jw_kT/cT}+e^{-2cT}-1\right)\Bigg\} \qquad (69b)$$

Using the fact that the noise $n_c(t)$ and $n_s(t)$ are independent over disjoint intervals and the random variables N_c and N_s are independent identically distributed (iid) Gaussian random variables with zero mean and the variance σ_i^2 computed from

(B.18) and given by (46), we can employ the variance as,

$$\sigma_i^2 = \frac{N_{sp} h_f (G-1) c}{4MGP} \qquad \text{as described in (46)} \tag{70}$$

b. Derivation of Probability Density Function

As it is explained in the first and second section as well, X_i is noncentral chi-square distributed with the following pdf also given in (47)

$$f_{X_i}(X_i) = \frac{1}{2\sigma_i^2} \left(\frac{x_i}{\psi^2} \right)^{M-1/2} e^{-(x_i+\psi^2)/2\sigma_i^2} I_{M-1} \left(\frac{\psi \sqrt{x_i}}{\sigma_i^2} \right) \tag{71}$$

where ψ^2 is described as in (69)

$$b_{0,0} = \sqrt{\frac{1}{(1+r)}} \quad \text{for} \quad \text{bit one} \tag{72}$$

$$b_{0,0} = \sqrt{\frac{r}{(1+r)}} \quad \text{for} \quad \text{bit zero} \tag{73}$$

$$\sigma_i^2 = \frac{N_{sp} h_f (G-1) c}{4MGP} \qquad \text{as in (46)} \tag{74}$$

The special case where the extinction ratio $r = 0$ introduces the chi-square pdf given by (52) and [18],

$$f_{x_0}(x_0) = \frac{1}{(M-1)!(2\sigma_0^2)^M} x_0^{M-1} e^{-x_0/2\sigma_0^2} \tag{75}$$

2. Bit Error Probability

For a detection threshold α and an ISI/ACI pattern $b = \{b_{0,i}, b_{k,\ell}\}$ where $i = -L_0, \cdots, 0$ and $k = -M/2, \cdots, M/2 (k \neq 0)$, the bit error probability is defined as in (53),

$$P_b(b) = \frac{1}{4} erfc \left(\frac{\alpha - x_0(b)}{\sqrt{2}\sigma_y} \right) + \frac{1}{4} erfc \left(\frac{x_1(b) - \alpha}{\sqrt{2}\sigma_y} \right) \tag{76}$$

where

$$\sigma_Y^2 = \sigma_W^2 = \frac{W_0}{T(RGP)^2} \tag{77}$$

Bit error probability for the worst case analysis and exact analysis are obtained by taking the expected value of $P_b(x_0, x_1)$ with respect to x_0 and x_1 by using (69a) and (69b), respectively.

P_b for the worst case analysis:

$$P_b = \frac{1}{4}\int_o^\infty erfc\left(\frac{\alpha - x_0(b)}{\sqrt{2}\,\sigma_Y}\right) f_{x_0}(x_0)dx_0 + \frac{1}{4}\int_0^\infty erfc\left(\frac{x_1(b) - \alpha}{\sqrt{2}\,\sigma_Y}\right) f_{x_1}(x_1)dx_1 \quad (78)$$

P_b for the exact analysis:

$$\begin{aligned} P_b \;=\; & \frac{1}{2\pi}\cdot\frac{1}{4}\int_0^\infty\int_0^{2\pi} erfc\left(\frac{\alpha - x_0(b,\phi)}{\sqrt{2}\,\sigma_Y}\right) f_{x_0}(x_0)d\phi dx_0 \\ & \frac{1}{2\pi}\cdot\frac{1}{4}\int_0^\infty\int_0^{2\pi} erfc\left(\frac{x_1(b,\phi) - \alpha}{\sqrt{2}\,\sigma_Y}\right) f_{x_1}(x_1)d\phi dx_1 \end{aligned}$$

The optimal threshold α that minimizes the bit error probability is the value that satisfies the following equation,

$$\int_0^\infty erfc\left(\frac{\alpha - x_0(b)}{\sqrt{2}\,\sigma_Y}\right) f_{x_0}(x_0)dx_0 = \int_0^\infty erfc\left(\frac{x_1(b) - \alpha}{\sqrt{2}\,\sigma_Y}\right) f_{x_1}(x_1)dx_1 \quad (79)$$

3. Numerical Results

In this section, we present the numerical results for the system employing the optical amplifier and the Fabry-Perot filter in the receiver model for multi-channel with the following parameters: bit rate R_b = 2.56 Gbps, optical amplifier gain G = 1000, free spectral range FSR = 3800 GHz, M = 3 and 4, channel spacing I = 8, 12, and c = 38.4 GHz. In our analysis, we consider that the signal is band-limited and incorporate the degradation caused by the signals in the nearest adjacent four channels. Since we deal with multi-channel in this section, we will see the effect of ISI and ACI components on the performance of the system, unlike the single channel case.

For the worst case analysis with optimum threshold, $b_{0,0} = 0$ for bit zero, $b_{0,0} = 1$ for bit one. Figure 18 shows the effect of ISI and ACI for $M = 3$, $cT = 15$, and $I = 8, \infty$ in terms of bit error probability and input power (dBW). As can be seen from the graph, the single channel requires -68.8 dBW in order to be able to achieve bit error probability $P_b = 10^{-15}$. The system with ISI but no ACI, requires -67.5 dBW to achieve the same bit error probability, which corresponds to a 1.3 dBW power penalty as compared to the single channel case. When the adjacent channels are taken into account for channel spacing $I = 12$ and 8, the power penalties are 3.8 and 6.0 dBW, respectively. As the channel spacing between channels gets larger, the effect of ACI becomes less significant.

Figures 19 and 20 show the effect of the value of M, which is the ratio of bit duration (T) to the time constant of the filter impulse response (T'). As explained in section 2, the noise variance has a dependency on M as given in (46),

$$\sigma_i^2 = \frac{N_{sp} h f (G-1)}{4MGP}$$

A M decreases, the noise variance gets larger and more noise power is obtained accordingly. As can be seen from the figures, more input power is required for $M = 3$ rather than $M = 4$ at $P_b = 10^{-15}$ as expected from the results obtained in the single channel case in section 2.

When we compare the worst case analysis and exact analysis with each other, as we expected, exact analysis requires slightly less power than worst case analysis in order to obtain the same probability of bit error $P_b = 10^{-15}$ as shown in Fig. 21.

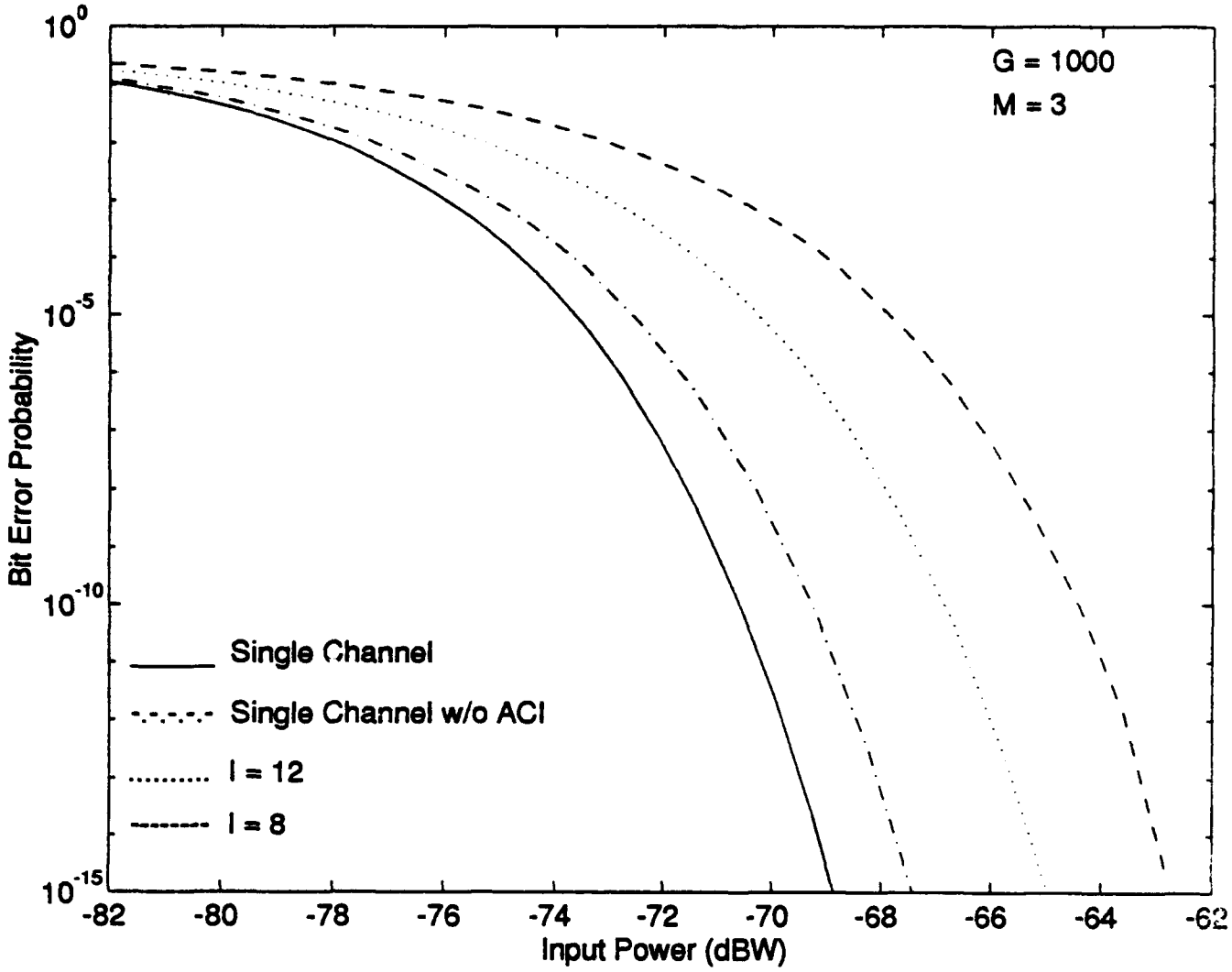

Figure 18: Bit error probability versus input power for Fabry-Perot filter with $G = 1000$, $M = 3$, $W_0 = 10^{-12}$ A^2/Hz (multichannel worst case analysis).

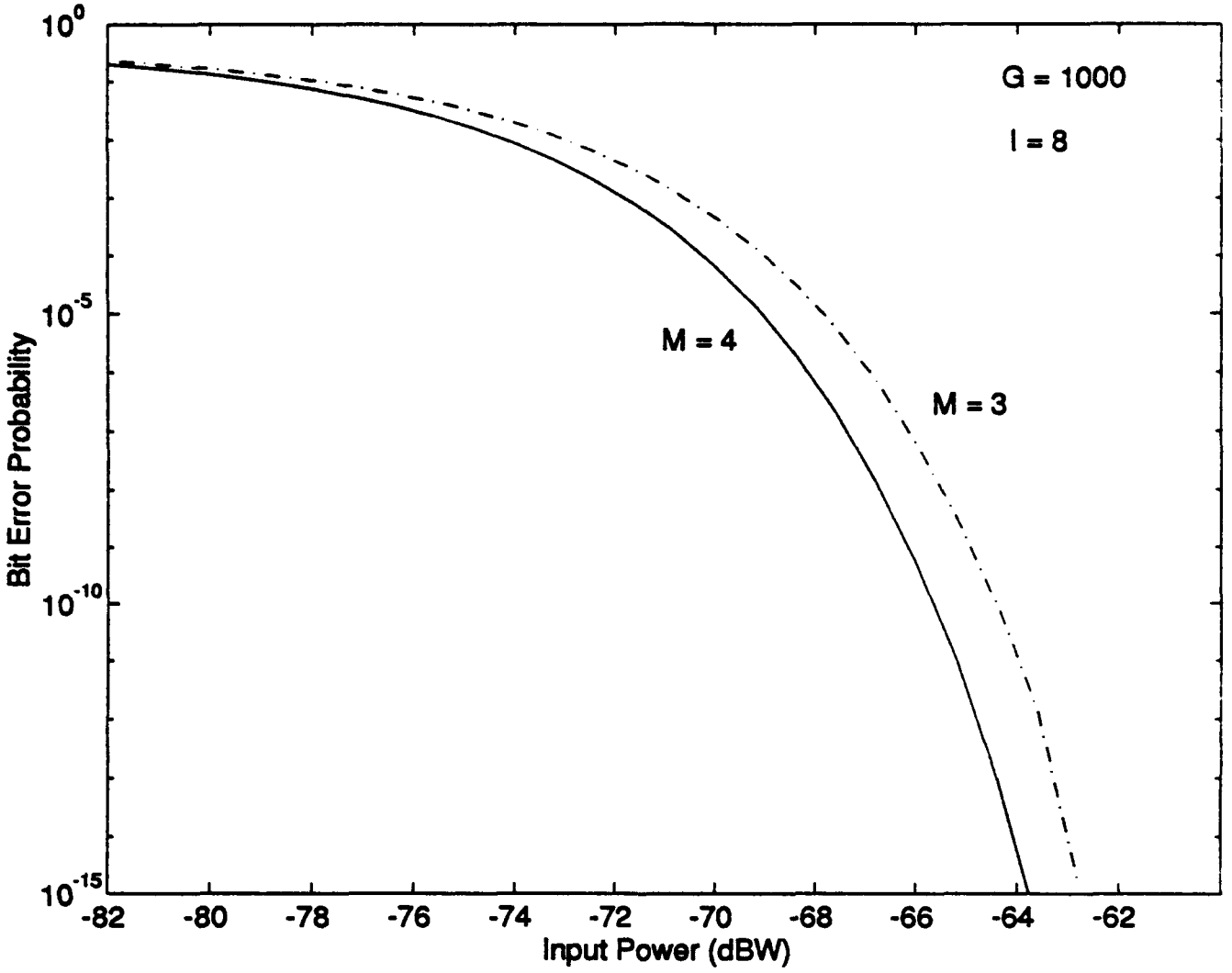

Figure 19: Bit error probability versus input power for a Fabry-Perot filter as a function of M with $G = 1000$, $W_0 = 10^{-23}$ A^2/Hz, $I = 8$.

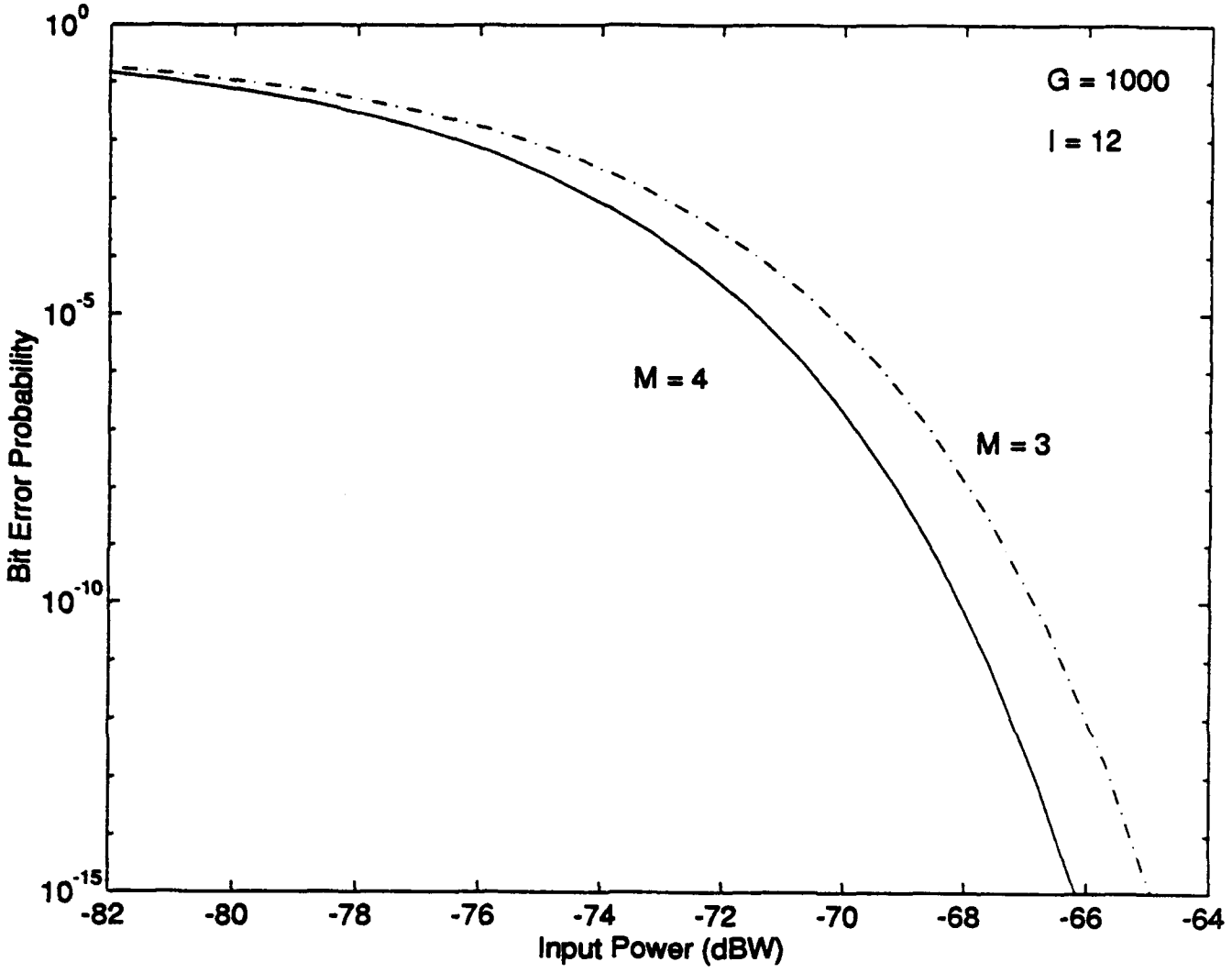

Figure 20: Bit error probability versus input power for a Fabry-Perot filter as a function of M with $G = 1000$, $W_0 = 10^{-23}$ A^2/Hz and $I = 12$.

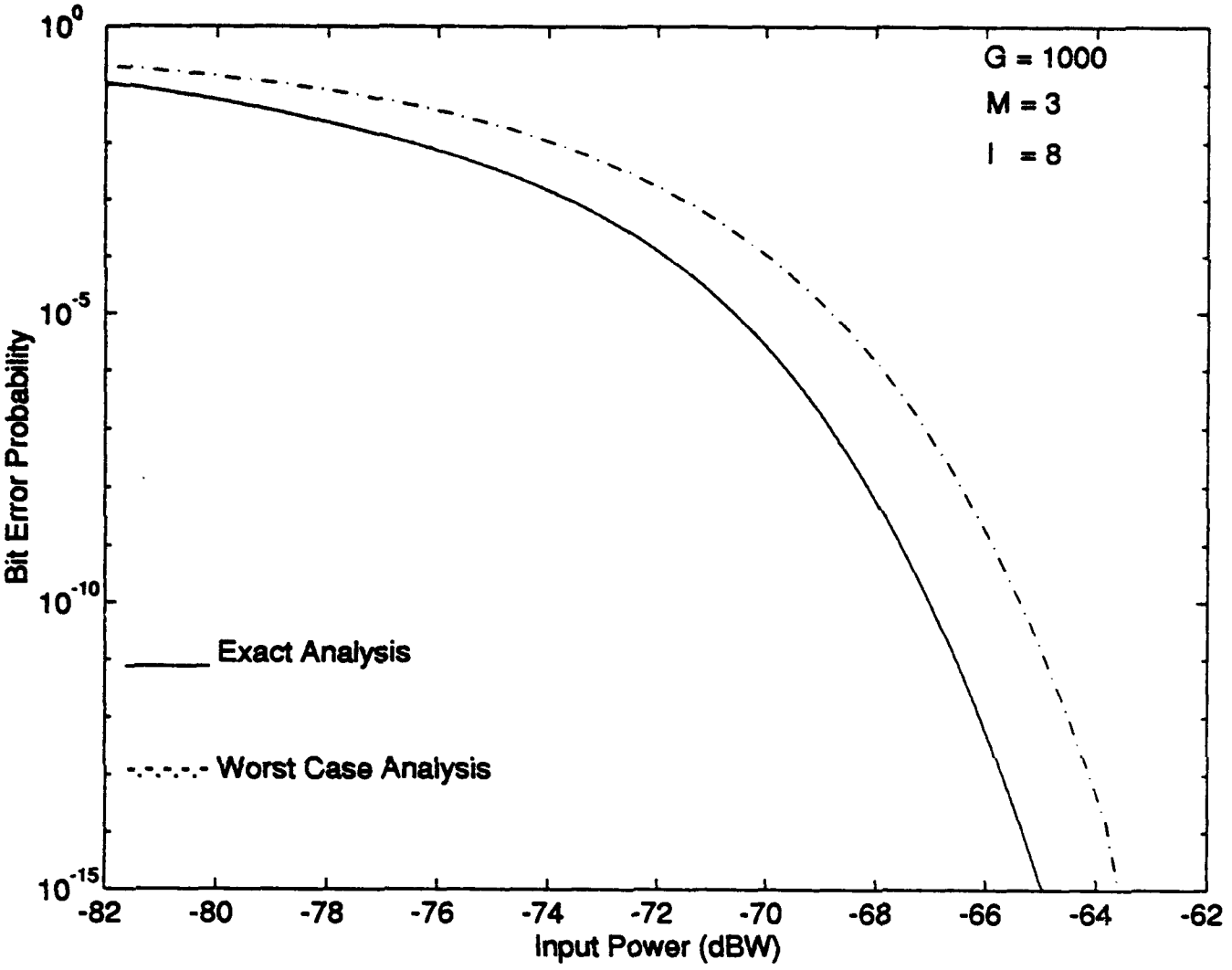

Figure 21: Bit error probability versus input power for Fabry-Perot filter with $G = 1000$, $W_0 = 10^{-23}$ A^2/Hz, $M = 3$, $I = 8$ (comparison between exact and worst case analysis for multichannel).

[THIS PAGE INTENTIONALLY LEFT BLANK]

III. CONCLUSIONS

We have presented a detailed analysis of direct detection lightwave systems employing an optical preamplifier at the receiver and derived the closed form expression for the bit error probability of WDM systems employing on-off (OOK) as a modulation format. We have considered various cases in which the receiver model uses either a finite-time integrator or Fabry-Perot filter operating in a single channel or multi-channel environment. We have taken into account the optical amplifier noise, the postdetection receiver noise, the shot noise, and the effect of the nonzero laser linewidth.

For the finite-time integrator, we conclude that the amplifier noise effect is most pronounced at low postdetection thermal noise. A larger gain amplifier should be used when the postdetection thermal noise is dominant, while a smaller gain amplifier should be used when the postdetection thermal noise is small and amplifier noise dominates.

The performance of the system employing the Fabry-Perot filter in a single channel environment depends on the value of M, which is defined as the ratio of bit duration to time constant of the impulse response of the filter. When we chop the filter impulse response at a high value of T', which requires a small value of M based on the relation M and T' for a constant bit rate ($M = T/T'$), we conclude that more power is required to achieve the $P_b = 10^{-15}$ than chopping the impulse response at a lower value of T'. The reason for this is that the noise variance of the Fabry-Perot filter is inversely proportional to the value of M. As M decreases, more power penalty is paid to obtain the same bit error probability.

When we compare the system employing a finite-time integrator and the system employing a Fabry-Perot filter, we conclude that the finite-time integrator has better performance with a high gain amplifier under low thermal noise values than the Fabry-Perot filter when we chop the impulse response of the filter at a high value of T'. For a larger value of M, we conclude that the Fabry-Perot filter has better performance with a high gain amplifier and low thermal noise values than the finite-time integrator.

The system employing an optical preamplifier and a Fabry-Perot filter in a multi-channel environment suffers from intersymbol interference and adjacent channel interference. When the channel spacing is large, the effect of ACI is small.

APPENDIX A

Derivation of the Expected Value $\overline{X}_i = E\{X_i\}$ [33]

Taking the expected of (4) we obtain

$$\overline{X}_i = \frac{E\{|s_i(t)|^2\}}{GP} = \frac{1}{T'^2GP} E\left\{\left|\int_{t-T'}^{T'} r_i(\tau)d\tau\right|^2\right\} \tag{A.1}$$

Substituting (1) into (A1) we have

$$\begin{aligned}\overline{X}_i &= \frac{1}{T'^2GP} E\left\{\left|\int_{t-T'}^{T'} \left[\sqrt{GP}\, b_i e^{j\theta(\tau)} + n_c(\tau) + jn_s(\tau)\right] d\tau\right|^2\right\} \\ &= \frac{b_i^2}{T'^2}\int_{t-T'}^{T'}\int_{t-T'}^{T'} E\left\{e^{j[\theta(\tau_1)-\theta(\tau_2)]}\right\} d\tau_1 d\tau_2 + \frac{N_{sp}hf(G-1)}{T'GP}\end{aligned} \tag{A.2}$$

The laser phase noise $\theta(t)$ is characterized by a Wiener process [16] such that its derivative is a zero mean white Gaussian process of PSD $2\pi\beta$ where β is the laser linewidth. The variance of $\theta(t)$ is $2\pi\beta t$ and it can be shown that

$$E\left\{e^{j[\theta(\tau_1)-\theta(\tau_2)]}\right\} = e^{-\pi\beta|\tau_1-\tau_2|} \tag{A.3}$$

Substituting (A.3) into (A.2) yields

$$\overline{X}_i = \frac{2M^2b_i^2}{(\pi\beta T)^2}\left(\frac{\pi\beta T}{M} + e^{-\pi\beta T/M} - 1\right) + \frac{MN_{sp}hf(G-1)}{TGP} \tag{A.4}$$

[THIS PAGE INTENTIONALLY LEFT BLANK]

APPENDIX B

Derivation of X_i and G_i

X_i is the squared envelope signal detected by photodetector with responsivity R and scaled by $1/TRGP$. It is defined as in (4)

$$X_i = \frac{1}{TRGP}\int_0^T R|S_i(t)|^2 dt \tag{B.1}$$

$$S_i(t) = S_B(t) = \sqrt{GP}\, b_{0,0}\int_0^t h(t-\tau)d\tau \tag{B.2}$$

$$h(t) = ce^{-ct}, \qquad t > 0 \tag{B.3}$$

$$S_i(t) = \sqrt{GP}\, b_{0,0}\left(1-e^{-ct}\right), \qquad 0 < t \le T \tag{B.4}$$

$$X_i = \frac{1}{TRGP}\int_0^T R\left|\sqrt{GP}\, b_{0,0}\left(1-e^{-ct}\right)\right|^2 dt \tag{B.5}$$

$$X_i = b_{0,0}\left(1-\frac{2}{cT}\left(1-e^{-cT}\right)+\frac{1}{2cT}\left(1-e^{-2cT}\right)\right) \tag{B.6}$$

It is described in the first section, the noise $n_c(t)$ and $n_s(t)$ are independent over disjoint intervals and the random variables N_{ck} and N_{sk} are independent identically distributed Gaussian random variables with zero mean. Their variances in (46) can be computed as follows,

$$N_c(t) = \frac{1}{\sqrt{MGP}}\int_{-\infty}^t h(t-\tau)n_c(\tau)d\tau \tag{B.7}$$

$$h(t) = h_\infty(t)p_{T'}(t) \tag{B.8}$$

$$p_{T'}(t) = \begin{cases} 1 & 0 < t < T' \\ 0 & \text{otherwise} \end{cases} \tag{B.9}$$

$$N_c(t) = \frac{1}{\sqrt{MGP}}\int_{-\infty}^t h_\infty(t-\tau)n_c(\tau)p_{T'}(t-\tau)d\tau$$

$$= \frac{1}{\sqrt{MGP}}\int_{t-T'}^t h_\infty(t-\tau)n_c(\tau)d\tau$$

$$N_c(nT') = \frac{1}{\sqrt{MGP}} \int_{(n-1)T'}^{nT'} h_\infty(nT' - \tau) n_c(\tau) d\tau \tag{B.10}$$

$$n_c(\tau) = \frac{N_0}{2} \tag{B.11}$$

$$\sigma_{N_c}^2 = \sigma_{N_s}^2 = \frac{N_0}{2MGP} \int_{(n-1)T'}^{nT'} h_\infty^2(nT' - \tau) d\tau \tag{B.12}$$

using $\tau' = nT' - \tau$,

$$\begin{aligned} \sigma_{N_c}^2 = \sigma_{N_s}^2 &= \frac{N_0}{2MGP} \int_{T'}^{0} h_\infty^2(\tau')(-d\tau') \\ &= \frac{N_0}{2MGP} \int_0^{T'} h_\infty^2(\tau) d\tau < \frac{N_0}{2MGP} \int_0^{\infty} h_\infty^2(\tau) d\tau \end{aligned}$$

$$\sigma_{N_c}^2 = \sigma_{N_s}^2 = \frac{N_o}{2MGP} \mathcal{E} \tag{B.13}$$

where

$$\mathcal{E} = \int_0^{T'} h_\infty^2(\tau) d\tau \tag{B.14}$$

If we use the approximated RC filter of which impulse response $h(t)$ given as in (B.3)

$$\sigma_{N_c}^2 = \sigma_{N_s}^2 = \frac{N_0 \mathcal{E}}{2MGP} \tag{B.15}$$

where

$$\begin{aligned} \mathcal{E} &= \int_0^{T'} h_\infty^2(t) dt \\ &= \int_0^{T'} (ce^{-ct})^2 dt \\ \mathcal{E} &= \frac{c}{2}(1 - e^{-2cT'}) \end{aligned} \tag{B.16}$$

We can approximate $\mathcal{E}$ as $c/2$ since the exponential term goes to zero due to the high value of $2cT'$.

$$\mathcal{E}_\infty \approx \frac{c}{2} \tag{B.17}$$

Finally, the variable is found as

$$\sigma_{N_c}^2 = \sigma_{N_s}^2 \approx \frac{N_0}{2MGP} \cdot \frac{c}{2}$$
$$\sigma_{N_c}^2 = \sigma_{N_s}^2 \approx \frac{N_{sp} h_f (G-1) c}{4MGP} \tag{B.18}$$

We also know that this variance value can be represented by

$$\sigma_{N_c}^2 = \sigma_{N_s}^2 = \sigma_i^2 \quad \text{in pdf (54)} \tag{B.19}$$

where N_{sp} (the spontaneous emission factor) is unity and

$$c = \frac{FSR(1-\rho)}{\rho} \tag{B.20}$$

[THIS PAGE INTENTIONALLY LEFT BLANK]

APPENDIX C

Data signal in channel k:

$$b_k(t) = \sum_{\ell=-L}^{0} b_{k,\ell} e^{jw_k t} p_T(t - \ell T) \tag{C.1}$$

Data signal in channel 0:

$$b_0(t) = \sum_{i=-L_0}^{0} b_{0,i} p_T(t - iT) \tag{C.2}$$

Bit in channel k in L^{th} time interval $(\ell T, (\ell + 1)T)$

$$b_{k,\ell} \in \{0, e^{j\phi_k}\}$$

Bit in channel ϕ in i^{th} time interval $(iT, (i + 1)T)$

$$b_{0,i} \in \{0, 1\}$$

Detected bit in $(0, T)$

$$b_{0,0} \in \{0, 1\}$$

depending on where bit zero or bit one is present.

Desired channel = channel 0

Adjacent channel = channel k, where

$$k = -\frac{M}{2}, \cdots, -1, 1, \cdots, \frac{M}{2}, M \text{ even integer}$$

w_k = Frequency spacing between channel k and channel 0

$$w_k = \frac{2\pi k I}{T} \tag{C.3}$$

ϕ_k = Phase offset between channel k and channel 0 uniformly distributed over $(0, 2\pi)$

$$p_T(t) = \begin{cases} 1 & 0 \le t \le T \\ 0 & \text{otherwise} \end{cases}$$

$$p_T(t - iT) = \begin{cases} 1 & iT \le t \le (i + 1)T \\ 0 & \text{otherwise} \end{cases} \tag{C.4}$$

The received signal at the output of the preamplifier and at the input of the Fabry-Perot filter (for channel ϕ)

$$r(t) = \sqrt{GP}\, b_0(t) + \sum_{\substack{k=-M/2 \\ k\neq 0}}^{M/2} \sqrt{GP}\, b_i(t) \tag{C.5}$$

where P is the optical power and G is the optical amplifier gain.

The output of the Fabry-Perot filter is

$$r_0(t)_0 \int_{-\infty}^{\infty} h(t-\tau) r(\tau) d\tau \tag{C.6}$$

where $h(t)$ is the equivalent lowpass impulse response of the Fabry-Perot filter of channel 0,

$$h(t) = ce^{-ct} \qquad t > 0 \tag{C.7}$$

$$\begin{aligned} r_0(t) &= \sqrt{GP} \int_{-\infty}^{\infty} h(t-\tau) b_0(\tau) d\tau + \sqrt{GP} \sum_{\substack{k=-M/2 \\ k\neq 0}}^{M/2} \int_{-\infty}^{\infty} h(t-\tau) b_k(\tau) d\tau \\ &= \sqrt{GP}\, b_{0,0} \int_{-\infty}^{\infty} h(t-\tau) p_T(\tau) d\tau \\ &\quad + \sqrt{GP} \sum_{i=-L_0}^{-1} b_{0,i} \int_{-\infty}^{\infty} h(t-\tau) p_T(\tau - iT) d\tau \\ &\quad + \sqrt{GP} \sum_{\substack{k=-M/2 \\ k\neq 0}}^{M/2} \sum_{\ell=-L}^{0} b_{k,\ell} \int_{-\infty}^{\infty} h(t-\tau) e^{jw_k\tau} p_T(\tau - \ell T) d\tau \end{aligned} \tag{C.8}$$

Since we are interested only in the detection interval $0 < t < T$, we need to evaluate $S(t) = r_0(t)$, $0 < t \leq T$

$$\begin{aligned} S(t) &= \sqrt{GP}\, b_{0,0} \int_0^t h(t-\tau) d\tau + \sqrt{GP} \sum_{i=-L_0}^{-1} b_{0,i} \int_{iT}^{(i+1)T} h(t-\tau) d\tau + \sqrt{GP} \sum_{\substack{k=-M/2 \\ k\neq 0}}^{M/2} \\ &\left(\left[\sum_{\ell=-L}^{-1} b_{k,\ell} \int_{\ell T}^{\ell+1)T} h(t-\tau) e^{jw_k\tau} d\tau \right] + b_{k,0} \int_0^t h(t-\tau) e^{jw_k\tau} d\tau \right) \end{aligned} \tag{C.9}$$

$$S(t) = S_B(t) + S_{ICI}(t) + S_{ACI}(t) \tag{C.10}$$

where

$$S_B(t) = \sqrt{GP}\, b_{0,0} \int_0^t h(t-\tau)d\tau \tag{C.11}$$

$$S_{ISI}(t) = \sqrt{GP} \sum_{i=-L_0}^{-1} b_{0,i} \int_{iT}^{(i+1)T} h(t-\tau)d\tau \tag{C.12}$$

$$S_{ACI}(t) = \sqrt{GP} \sum_{\substack{k=M/2 \\ k\neq 0}}^{M/2} \left(\left[\sum_{\ell=-L}^{-1} b_{k,\ell} \int_{\ell T}^{(\ell+1)T} h(t-\tau)e^{jw_k\tau}d\tau \right] \right.$$

$$\left. + b_{:,0} \int_0^t h(t-\tau)e^{jw_k\tau}d\tau \right) \tag{C.13}$$

The evaluation of the integrals are as follows

$$S_B(t) = \sqrt{GP}\, b_{0,0}(1-e^{-ct}), \qquad 0 < t < T \tag{C.14}$$

$$S_{ISI}(t) = \sqrt{GP} \sum_{i=-L_0}^{-1} b_{0,i} \left(e^{(i+1)cT} - e^{icT} \right), \qquad 0 < t < T \tag{C.15}$$

$$S_{ACI}(t) = \sqrt{GP}\, ce^{-ct} \sum_{\substack{k=-M/2 \\ k\neq 0}}^{M/2} \frac{1}{c+jw_k}$$

$$\left(\left[\sum_{\ell=-L}^{-1} b_{k,\ell} \left(e^{(c+jw_k)(\ell+1)T} - e^{(c+jw_k)T} \right) \right] + b_{k,0} \left(e^{(c+jw_k)t} - 1 \right) \right) \tag{C.16}$$

Worst Cast Analysis

$b_{0,i} = b_-,\ L_0 = \infty$

$$S_{ISI}^{wc}(t) = \sqrt{GP}\, b_- e^{-ct} \qquad 0 < t \leq T \tag{C.17}$$

$b_{k,\ell} = b_{k,0} = b,\ L = \infty$

$$S_{ACI}^{wc}(t) = \sqrt{GP}\, b \sum_{\substack{k=-M/2 \\ k\neq 0}}^{M/2} \frac{e^{jw_k t}}{1 + \frac{jw_k}{c}} \qquad 0 < t \leq T \tag{C.18}$$

with I = integer > 0 and $w_k = 2\pi kI/T$,

$$X = R \int_0^T |S_i(t)|^2 dt \tag{C.19}$$

By using (C.14), (C.17), and (C.18), the evaluation of integrals gives the value of X as

$$\begin{aligned} X \;=\; & \frac{1}{TRGP}\Bigg[TRGP\Bigg(b_{0,0}^2\left[1 - \frac{2}{cT}(1 - e^{-cT}) + \frac{1}{2cT}(1 - e^{-2cT})\right] \\ & + b_-^2\left[\frac{1}{2cT}(1 - e^{-2cT})\right] + b_{0,0}b_-\left[\frac{1}{cT}(1 - 2e^{-cT} + e^{-2cT})\right] \\ & + \Bigg[|b|^2 + \frac{2}{cT}(1 - e^{-cT})Re\{b\}(b_- - b_{0,0}) \\ & \cdot \sum_{\substack{k=-M/2 \\ k\neq 0}}^{M/2} \frac{1}{1 + \left(\frac{w_k}{c}\right)^2}\Bigg]\Bigg)\Bigg] \end{aligned} \tag{C.20}$$

REFERENCES

[1] Special issue on optical amplifiers, *J. Lightwave Technol.*, Vol. 9, No. 2, Feb. 1991.

[2] N. A. Olsen, "Lightwave systems with optical amplifiers," *J. Lightwave Technol.*, Vol. 7, No. 7, pp. 1071–1082, July 1989.

[3] S. D. Personick, "Applications for quantum amplifiers in simple digital optical communication systems," *Bell Syst. Tech. J.*, Vol. 52, No. 1, pp. 117–133, Jan. 1973.

[4] Y. Yamamoto, "Noise and error rate performance of semi-conductor laser amplifiers in PCM-IM optical transmission systems," *IEEE J. Quantum Electron.*, Vol. 16, pp. 1073–1081, 1980.

[5] O. K. Tonguz, "Impact of spontaneous emission noise on the sensitivity of direct detection lightwave receivers using optical analyzers," *Electron. Lett.*, Vol. 27, No. 16, pp. 1343–1344, Aug. 1990.

[6] O. K. Tonguz and L. G. Kazovsky, "Theory of direct detection lightwave receivers using optical amplifiers," *J. Lightwave Technol.*, Vol. 9, No. 2, pp. 174–181, Feb. 1991.

[7] T. Li and M. C. Teich, "Bit error rate for a lightwave communication system incorporating an erbrium-doped fiber amplifier," *Electron. Lett.*, Vol. 27, No. 7, pp. 598–600, Mar. 1991.

[8] D. Marcuse, "Derivation of analytical expressions for the bit error probability in lightwave systems with optical amplifiers," *J. Lightwave Technol.*, Vol. 8, No. 12, pp. 1816–1823, Dec. 1990.

[9] D. Marcuse, "Calculation of bit error probability for a lightwave system with optical amplifiers and post detection Gaussian noise," *J. Lightwave Technol.*, Vol. 9, No. 4, pp. 505–513, Apr. 1991.

[10] P. A. Humblet and M. Azizoglu, "On the bit error rate of lightwave systems with optical amplifiers," *J. Lightwave Technol.*, Vol. 9, No. 11, pp. 1576–1582, Nov. 1991.

[11] P. S. Henry, "Error rate performance of optical amplifiers," Optical Fiber Communications Conference, Tech. Digest, paper THK3, Feb. 1989.

[12] A. Yariv, *Optical Electronics.* New York: Holt, Rhinehart and Winston, 1985.

[13] G. J. Foschini, L. J. Greenstein, and G. Vannucci, "Noncoherent detection of coherent lightwave signals corrupted by phase noise," *IEEE Trans. Commun.*, Vol. 36, No. 3, pp. 306–314, Mar. 1988.

[14] M. Azizoglu and P. A. Humblet, "Envelope detection of orthogonal signals with phase noise," *J. Lightwave Technol.*, Vol. 9, No. 10, pp. 1398–1410, Oct. 1991.

[15] J. R. Barry and E. A. Lee, "Performance of coherent optical receivers," *Proc. IEEE*, Vol. 78, No. 8, pp. 1369–1394, Aug. 1990.

[16] J. Salz, "Coherent lightwave communications," *AT&T Tech. J.*, Vol. 64, No. 10, pp. 2153–2209, Dec. 1985.

[17] A. Papoulis, *Probability, Random Variables, and Stochastic Processes.* New York: McGraw-Hill, 1985.

[18] J. G. Proakis, *Digital Communications*, 2nd Ed. New York: McGraw-Hill, 1989.

[19] L. W. Couch, II, *Digital and Analog Communication Systems*, 4th Ed. New York: McMillan, 1993.

[20] M. Azizoglu, "Phase noise in coherent optical communications," Ph.D. thesis, Massachusetts Institute of Technology, 1991.

[21] G. J. Foschini, G. Vannucci, and L. J. Greenstein, "Envelope statistics for filtered optical signals corrupted by phase noise," *IEEE Trans. Commun.*, Vol. 37, No. 12, pp. 1293–1302, Dec. 1989.

[22] G. L. Pierobon and L. Tomba, "Moment characterization of phase noise in coherent optical systems," *J. Lightwave Tech.*, Vol. 9, No. 8, pp. 996–1005, Aug. 1991.

[23] W. Feller, *An Introduction to Probability Theory and Its Applications*, Vol. II, 2nd Ed. New York: John Wiley & Sons, 1971.

[24] S. D. Personick, "Receiver design for digital fiber-optic communications systems, Part I," *Bell Systems Tech. J.*, No. 6, pp. 843–875, July–Aug. 1973.

[25] G. Jacobsen, "Multichannel system design using optical preamplifiers and accounting for the effects of phase noise, amplifier noise, and receiver noise," *J. Lightwave Technol.*, Vol. 10, No. 3, pp. 367–377, Mar. 1992.

[26] G. Jacobsen and I. Garrett, "The effect of crosstalk and phase noise in multichannel coherent optical ASK systems," *J. Lightwave Technol.*, Vol. 9, No. 8, pp. 1006–1018, Aug. 1991.

[27] L. G. Kazovsky, P. Meissner, and E. Patzak, "ASK multiport optical homodyne receivers," *J. Lightwave Technol.*, Vol. LT-5, No. 6, pp. 770–791, June 1987.

[28] J. I. Marcum, "Statistical theory of target detection by pulsed radar," *IEEE Trans. Inf. Theory*, Vol. IT-6, pp. 59–267, Apr. 1960.

[29] T-C. Chou, "A simple analytical model for dense WDM/OOK systems," M.S. Thesis, Naval Postgraduate School, 1994.

[30] W. H. Hamdy and P. A. Humblet, "Sensitivity analysis of direct detection optical FAMA networks with OOK modulation," *J. Lightwave Technol.*, Vol. 11, pp. 782–794, May/June 1993.

[31] C. S. Li, F. F. Tong, K. Liu, and D. G. Messerschmitt, "Channel capacity optimization of chip limited dense WDM/WDMA systems using OOK/FSK modulation and optical fibers," *J. Lightwave Technol.*, Vol. 10, No. 8, pp. 1148–1161, Aug. 1992.

[32] P. F. Green, Jr., *Fiber Optic Networks*, Englewood Cliffs, New Jersey, Prentice-Hall, 1993.

[33] T. T. Ha, Gerd E. Keiser, and Randy L. Borchardt, "Analysis of direct detection lightwave systems with optical amplifiers," MILCOM '94, Oct. 1994.

[THIS PAGE INTENTIONALLY LEFT BLANK]

INITIAL DISTRIBUTION LIST

		No. Copies
1.	Defense Information Center Cameron Station Alexandria, VA 22304-6145	2
2.	Library Code 52 Naval Postgraduate School Monterey, CA 93943-5101	2
3.	Chairman, Code EC Department of Electrical and Computer Engineering Naval Postgraduate School Monterey, CA 93943-5121	1
4.	Professor Tri T. Ha, Code EC/Ha Department of Electrical and Computer Engineering Naval Postgraduate School Monterey, CA 93943-5121	2
5.	Professor Randy L. Borchardt, Code EC/Bt Department of Electrical and Computer Engineering Naval Postgraduate School Monterey, CA 93943-5121	2
6.	Deniz Kuvvetleri Komutanligi Personel Daire Baskanligi Bakanliklar, Ankara, Turkey	1
7.	Deniz Harp Okulu Komutanligi Tuzla, Istanbul, Turkey	1
8.	Golcuk Tersanesi Komantanligi Golcuk, Kocaeli, Turkey	1

		No. Copies
9.	Taskizak Tersanesi Komutanligi Haskoy, Istanbul, Turkey	1
10.	Enver Kucukerman Ertugrul Mah. Necati Albruz Sok. Kucukerman Apt. No-12/27 Balmumcu, Istanbul, Turkey	2